Earthshine and the earth's albedo I: Earthshine observations and measurements of the lunar phase function for precise measurements of the earth's bond albedo

J. Qiu, E. Pallé, P.R. Goode, V. Yurchyshyn, J. Hickey, P. Montañés Rodriguez

Big Bear Solar Observatory, New Jersey Institute of Technology, Newark, NJ 07102, USA

M-C Chu

Department of Physics, The Chinese University of Hong Kong, Shatin N.T., Hong Kong

E. Kolbe

Department für Physik and Astronomie, Universität Basel, Basel, Switzerland

C.T. Brown, S.E. Koonin

W.K. Kellogs Radiation Laboratory, California Institute of Technology, Pasadena, CA 91125, USA

Abstract. We have been making sustained observations of the earthshine from Big Bear Solar Observatory in California since late 1998. We also have intermittent observations from 1994-5. We have re-invigorated and modernized a nearly forgotten way of measuring the earth's albedo, and hence its energy balance, previously studied by Danjon and his followers for about twenty-five years early in the last century, using their observations of the earthshine from France. This is the first in a series of papers covering observations and simulations of the earth's reflectance from photometric and spectral observations of the moon. Here, we develop a modern method of measuring, instantaneously, the large scale reflectance of the earth.

From California we see the moon reflecting sunlight from the third of the earth to the west of us in our evening – before midnight – which is during the moon's rising phase, and from the third of the earth to our east in our morning – after midnight – which is during the moon's declining phase.

We have precisely measured the scattering from the moon, as a function of lunar phase, which enables us to measure, in a typical night's observations, the earth's reflectance to an accuracy of 2.0% (equivalent to measuring the earth's emission temperature to ~ 0.8 K). The albedo is due to the interplay of cloud cover and the different landscapes.

1. Introduction

It is important to know whether there is an on-going global change in the earth's climate. To answer this, one needs precise, global/integrated measures of relevant quantities. The earth's climate is driven by the net sunlight deposited in the terrestrial atmosphere, and so, is critically sensitive to the solar irradiance and the earth's albedo. Precise measurements of the solar irradiance have been made by various satellites and by using ground-based proxies (for a review, see Fröhlich, 2000, and references therein). The spectrum of efforts to determine the earth's global albedo is not so rich. There have been efforts using systems of satellites (Buratti et al., 1996, and references therein), but virtually no efforts from the ground. Nonetheless, the earth's energy balance is determined in large part by its global albedo – the fraction of the incident sunlight that is directly reflected back into space without altering the internal energy budget of the atmosphere. The earth's surface, aerosols in the atmosphere and clouds all reflect some of the incoming solar short-wavelength radiation, preventing that energy from warming the planet. Further, about 13% of the solar radiation incident on the atmosphere is Rayleigh scattered, half of this reaching the earth's surface as diffuse radiation and the other half being returned to space (Houghton, 2002). Short-wavelength radiation, usually defined as having wavelengths between 0.15 and 4.0 μm, includes about 99% of the sun's radiation; of this energy, 46% is infrared (> 0.74 μm), 9% is ultraviolet (< 0.4 μm) and the remaining 45% is visible, with wavelengths between 0.4 and 0.74 μm (Liou, 2002). A significant portion of the solar energy is absorbed by the earth, where it drives terrestrial phenomena before being radiated back into space through the atmospheric window as infrared radiation peaking at about 10 μm.

The power going into the earth's climate system is

Copyright by the American Geophysical Union.

Paper number .
0148-0227/03/$9.00

$$P_{in} = C\pi R_e^2(1-A), \quad (1)$$

where C is the solar constant, R_e is the earth's radius and A is the short-wavelength Bond albedo (reflectance). Subsequently, this incoming power is re-radiated back into space at long-wavelengths, where

$$P_{out} = 4\pi R_e^2 \sigma \epsilon T_e^4, \quad (2)$$

where σ is the Stefan-Boltzmann constant and ϵ is the emissivity of the atmosphere (about 5.5 km high, where the long-wavelength radiation is emitted). T_e ($\sim 255K$) is the effective temperature of the earth defined by this equation with emissivity unit. One can relate that temperature to a more global climate parameter like the globally averaged surface temperature T_s. With this parameter, one must introduce an atmosphere effective emissivity, ϵ_a. Some publications refer to it as the normalized greenhouse effect g, following Ramanathan et al. (1989), with $g = 1 - \epsilon_a$. Then the outgoing power can be written as:

$$P_{out} = 4\pi R_e^2 \sigma (1-g) T_s^4, \quad (3)$$

If the planet is in radiative equilibrium, $P_{in} = P_{out}$, then we have

$$T_s^4 = \frac{C}{4\sigma(1-g)}(1-A). \quad (4)$$

This means that the Bond albedo, together with solar irradiance and the greenhouse effect, directly controls the earth's temperature. Global warming would result if either A decreased or g increased. The possibility of increasing greenhouse forcing due to an anthropogenic increase of atmospheric CO_2 over the past century, has been treated in detail in scientific literature over the past few decades (IPCC,1995; Houghton, 2002 and references therein). The scope of this paper, however, is the earth's short-wavelength albedo, which could also play a role. By measuring the earth's reflectance and the spectrum of the light reflected by the earth, one can determine A and g, respectively.

It has been known for some time that the so-called solar constant varies. In particular, data from the Active Cavity Radiometer (ACRIM I) on board the Solar Maximum Mission have shown for one cycle ($\sim$ 11 years) that the solar irradiance is about 0.1% greater at activity maximum than at activity minimum (Willson and Hudson 1988, 1991), and now this result from a series of satellites covers two solar cycles (Fröhlich, 2000). The precise origin of the changing irradiance is generally attributed to a competition between two components of the sun's magnetic field – dark sunspots and bright faculae, but an unambiguous description remains elusive. Based on climatological models of heat storage and thermal inertia of the oceans (Jayne and Marotzke,2001) it is widely accepted in the climate community that a 0.1% (0.3 Wm^{-2}) change is several times too small to be climatologically significant over the 11-year solar cycle (Lean, 1997), particularly if it is to be further obscured by a steady increase in greenhouse forcing. It has been suggested that there may have been two to three times larger, sustained excursions in the recent past (Lean, 1997), like during the "Maunder Minimum" (1650-1710) when a sunspot was rare (Eddy, 1976). Still, there is strong evidence of a solar cycle influence on climate going back more than 100,000 years (Ram and Stoltz, 1999). If the 0.1% increase in the mean solar irradiance between the mid-1980s and 1990 were typical, then one is led to consider more carefully the possibility of a variation in the earth's albedo. After all, the earth's reflectance seems to show considerable variation (Goode et al, 2001).

It is not unreasonable to expect that global changes in the earth's climate would be manifest in changes in the earth's albedo. Potential parameters affecting the albedo are volcanic eruptions, surface vegetation and/or desertification (Betts, 2000), snow and ice area coverage (Randall et al, 1994), and atmospheric constituents such as water vapor and clouds, greenhouse gases and aerosols (Cess et al, 1996; Ramanathan et al, 1989; Charlson et al, 1992). Albedo changes will be determined by the total effect of the changes in all these parameters. However, these changing parameters will bring along multiple climate feedbacks, which make assessing the exact change in albedo a hard task (Cess et al, 1996). During the past decades there have been some efforts to measure the earth's albedo from space. The Earth Radiation Budget Experiment (ERBE) instruments were flown on the ERBS, NOAA-9 and NOAA-10 satellites from 1985 to 1990. More recently, in 2000, the Clouds and the Earth's Radiant Energy System (CERES) instruments have begun taking measurements. In the near future the TRIANA mission wil also contribute by observing the earth's reflectance from deep-space. However, a long-term data series of the earth's albedo is difficult to obtain due to the complicated inter-calibration of the different satellite data and the long gaps in the series.

To derive ideally perfect measurements of the earth's reflectance it would be necessary to observe reflected radiances from the earth, from all points on the earth and at all angles. Therefore, all measurements from which albedo can be inferred require assumptions and/or modelling to derive a good measurement. The availability of different albedo databases and their inter-comparisons can help to constrain the assumptions necesary to derive estimates. In this sense, long-term ground measurements of the earth's albedo complementary to those from satellites, would be an advantage.

Here, we focus on a terrestrial determination of the earth's global albedo from an old, and largely forgotten method. That is, global albedo can be determined by measuring the amount of sunlight reflected from the earth and in turn, back to the earth from the dark portion of the face of the moon (the "earthshine" or "ashen light"). The most important historical program of earthshine measurements was carried out by Danjon (1928, 1954) from a number of sites in France. He used a "cat's-eye" photometer to produce a double image of the moon, allowing the visual comparison of the intensities of two well-defined patches of the lunar surface – one in sunlight and the other in earthshine – at various lunar phases. Using the "cat's-eye" mechanism, he stopped-down the light from the sunlit portion to match the brightness of the ashen portion. This differential measurement removed many of the uncertainties associated with varying atmospheric absorption and the solar constant, allowing Danjon to achieve his estimated uncertainty of roughly 5%, ignoring his appreciable systematic error from an incorrect determination of the moon's reflectivity. Our measurements

are about an order of magnitude more precise than his estimates, in large part because we have better measurement technologies. We have also solved the problem of the uncertainty in the scattering from the moon as a function of the phase of the moon (see section 4). At about 1% precision on individual nights, our terrestrial measurements of the earth's albedo have a precision comparable to that from satellites like the ones derived from ERBE datasets, of around the same value (ERBE Data Management Team, 1985) and to those of the CERES instrumentation, of around 1% (Seiji et al, 2002).

From 1926 to 1930, Danjon made 207 measurements of earthshine. Dubois (1947) continued the program through 1960 from the observatory at Bordeaux using a Danjon-type photometer.

Danjon's and Dubois' results show a number of interesting features. The daily mean values of the observations vary more widely than would be expected on the basis of the variation of measurements on a single night. This can plausibly be attributed to daily changes in cloud cover. The typical lifetime of large scale cloud systems (1000's of km) is 3 days (Ridley, 2001), but from one night to the next the earth's area contributing to the earthshine changes (see Figure 1). Unfortunately, extensive cloud-cover data were not available at the time of Danjon's and Dubois' observations.

Danjon (1928) also examined his observations to determine whether there was a long-term trend in albedo, but found none. Dubois' observations for some 20 years ending in 1960, showed considerable annual variability, which he speculated was due to solar activity. His published monthly variations from 1940-1944 also show a strong correlation with the 1941-42 El Niño. In the past forty years, there have been observations of earthshine by Huffman et al. (1989) and one-time observations by Franklin (1967) and Kennedy (1969).

Danjon used his observations to estimate the mean global albedo. Since the observations are only at visible wavelengths, they must be corrected for the balance of the short-wavelength radiation, most of which is in the near IR. Estimates of this correction were made by Fritz (1949), after taking into account the decrease of the earth's albedo with increasing wavelength (our "blue planet"). Fritz also attempted to correct for the geographical bias in Danjon's observations. The earth western hemisphere (Asia, Russia), which was most frequently observed by Danjon, has a greater fraction of land than does the globe as a whole, implying that Danjon's value would be high because the sea is dark compared to land. Combining the decreases from the absence of the IR and geographical bias, Fritz found that Danjon's visual albedo of 0.40 corresponds to a Bond albedo (considering all the wavelengths and directions) of 0.36.

Flatte et al. (1991) noted that a correction must be made for the "opposition effect" present in lunar reflectance properties. Observations of the moon show that the moon's reflectivity has a strong angular dependence, which was unknown in Danjon's time. Hapke (1971) mentions in his review that the increase in brightness may be as much as 50 to 100 % for lunar phases angles from 5° to 0° (exact backscattering). This enhancement was once thought to be due to the porous nature of the lunar surface (Hapke, 1971), and was unknown in Danjon's time. More modern work has shown it to be caused by both coherent backscatter of the lunar soil and shadow hiding in roughly equal amounts (Hapke et al, 1998; Hapke et al, 1993; Helfenstein et al, 1997). The smallest lunar phase angle measured by Danjon was only 11°. The extent of the small-angle rise varies over different regions of the lunar surface, but can easily be the 20% required to reduce Fritz's value of 0.36 to the generally recognized standard of about 0.30 (Buratti et al., 1996). In fact, we shall see in section 4 that an incorrect lunar phase function is the primary source of Danjon's overly large visual albedo.

We have been steadily observing the earthshine from Big Bear since 1998 to determine the earth's reflectance and its variations. In this paper, we discuss in detail the method we used to determine reflectance from earthshine. As mentioned, the first such observations were made by Danjon (1928), and considerable modernization was required to make this method sufficiently precise to usefully complement satellite measurements. Beyond developing the methodology, our purpose here is to demonstrate the reliability of the technique. This is the first of a series of papers deriving from our earthshine project. The next two papers (Goode et al, 2003; Pallé et al, 2003) will present and interpret the results of our observational work and simulations of the observations. A fourth paper in preparation concerns our observations of the spectrum of the earthshine in the visible range (500-800 nm) from the $60''$ (1.5 m) telescope on Mt. Palomar, with a resolving power of $R = 19,000$.

In the following section we will discuss the theoretical approach to the earthshine Bond albedo determination. Section 3 describes in detail the data reduction techniques followed to analyze the earthine data. In section 4 our method for lunar phase function determination and the corrections applied to its calculation are also detailed. Finally, section 5 discusses the precision archieved in our nightly albedo determination. Two appendices have been included in the paper, the first deals with the optical setup of our telescope, and the observational technique followed during observations. The second contains the description of the two methods employed to determine the exact transmission of the filter used for our lunar bright side observations.

2. Determining the Earth's Reflectivity from Earthshine

Ground-based measurements of the short-wavelength (visible light and near infrared) albedo of a planet in our solar system are relatively straightforward – except for the earth. However, we can determine the albedo from the ground by measuring the earthshine. From a terrestrial perspective, the earthshine is the sunlight reflected from the day side of the earth to the moon, and finally back to an observer on the night side of the earth. At any moment, the earthshine can provide an instantaneous, differential cross-section of the sunlight reflected from the earth, see Figure 1.

The earth's differential cross-section depends on its geometrical albedo and its phase function. The geometrical albedo is independent of β, the earth's phase angle; rather, it is proportional to the backscattered cross-section. At the top of the atmosphere (taken by convention as being 30 km high by the ERBE data processing), the differential cross-section of the reflected sunlight for scattering by an angle β (note that β is the supplement of the usual scattering angle) is given by

$$\frac{d\sigma}{d\Omega} \equiv p_e f_e(\beta) R_e^2, \tag{5}$$

where R_e is the radius of the earth, p_e is the geometrical albedo of the earth and $f_e(\beta)$ is the earth's phase function, defined such that $f_e(0) = 1$, as can be seen in the Lambertian limit from Equation (8).

Using Equation (5), we can write the total scattering cross section as

$$\sigma = \int \frac{d\sigma}{d\Omega} d\Omega = \pi R_e^2 p_e \int_{-\pi}^{\pi} f_e(\beta) \mid \sin(\beta) \mid d\beta, \qquad (6)$$

where p_e and f_e depend on the earth's weather, season and climate. Additionally, f_e depends on the earth's phase as seen from the moon. From the total cross-section, we can define the Bond albedo – the fraction of solar energy incident on the planet that is reflected as

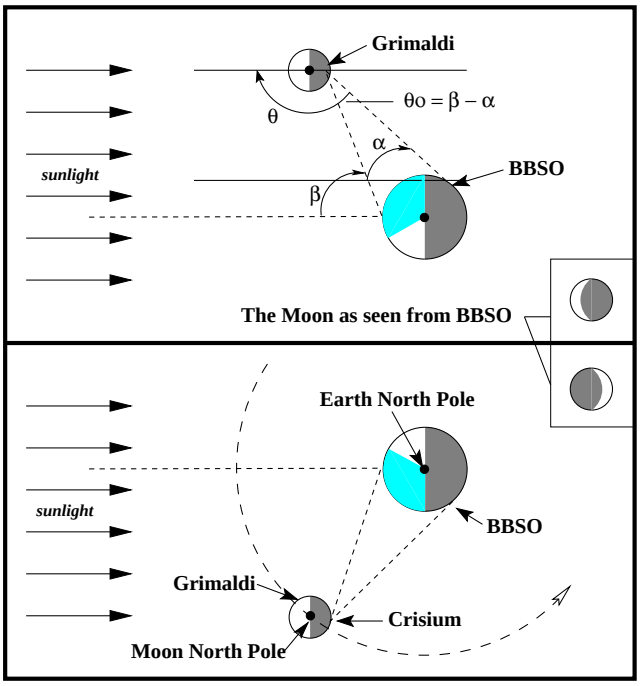

Figure 1. A not-to-scale cartoon of the sun-earth-moon system viewed from the pole of earth's orbit. In the top panel, the earth's topocentric phase angle, α, with respect to BBSO is defined. The plot also shows the moon's selenographic phase angle, θ, with respect to one of the fiducial points (Grimaldi) used in the observations made from BBSO (also indicated). β is the angle between the sunlight that is incident somewhere on the earth and reflected, as earthshine, to Grimaldi. $\theta_0 (= \beta - \alpha)$ is the angle between the earthshine that is incident, and reflected from the moon. The path of the earthshine is indicated by the arrows. θ_0 is of order 1°, or less. In the lower panel the same diagram is drawn for a negative lunar phase angle, and extra features like the moon's orbit around the earth are indicated. On both panels the aspect of the moon as would be seen from BBSO is also indicated in a box. The light-shaded areas of the earth indicate the aproximate latitude range that contributes to the earthshine. Note how for positive lunar phases (top panel) the earthshine contribution comes from latitudes west of BBSO while for negative phase (lower panel) angles it comes from latitudes east of BBSO.

$$A = \frac{\sigma}{\pi R_e^2} = p_e \int_{-\pi}^{\pi} f_e(\beta) \mid \sin(\beta) \mid d\beta. \qquad (7)$$

Using earthshine data, we integrate over the phases of the moon to determine, say, a seasonally or yearly averaged Bond albedo. β varies between 0 and $\pm\pi$, with 0 to π being the waning moon and -π to 0 being the waxing moon. This integration is done over a series of measurements, which comprise a wide range of geographical and temporal coverage. For example, for a few consecutive days of observation the coast of China may be present in all measurements, but its maximum contribution to the earthshine may come before, during, or after the time of our measurements. On the other hand, for a different night China may not be visible at all while Europe is. However, since we are averaging over a wide range of mixed surface types, the anisotropic reflective properties of individual elements may be masked, and the assumption of isotropy reasonable (Ueno, 1981). Thus, we can average our observations to derive reliable Bond albedo estimates on seasonal or yearly time scales.

If we assume that the earth is a Lambert sphere, we can do the integrals in Equations (6) and (7) exactly. A Lambert sphere isotropically reflects from its surface, which is assumed to be fully diffusive. Then, f_L, the earth's Lambert phase function, is determined by

$$f_L(\beta) = \frac{(\pi - \mid \beta \mid) \cos\beta + \sin \mid \beta \mid}{\pi}. \qquad (8)$$

The earth's phase function is observed to be very roughly Lambertian for $\mid \beta \mid \leq \frac{2\pi}{3}$, Goode et al. (2001). Under this assumption, we determine a simple proportionality between the geometric albedo and the global or Bond albedo, namely,

$$p_{e,L} = \frac{2}{3} A_{B,L}. \qquad (9)$$

Modelling confirms that the earth's phase function is approximately Lambertian for $\mid \beta \mid \leq \frac{2\pi}{3}$ (Flatte et al, 1991). Thus, a conveniently normalized, differential measure of the earth's reflectivity is the effective albedo, A^*, where

$$A^* \equiv \frac{p_e f_e}{p_{e,L} f_{e,L}} A_{B,L} = \frac{3}{2} \frac{p_e f_e}{f_{e,L}}, \qquad (10)$$

which is the albedo of a Lambert sphere that would give the same instantaneous reflectivity as the true earth at the same phase angle, and where an unchanged A^* as a function of phase angle would imply a Lambertian earth.

An observer on the moon in the region illuminated by the sun and visible from the earth would see both the direct sunlight and some part of the sunlit earth. The solar flux (or irradiance) seen by that observer would be

$$I_s = \frac{C}{R_{ms}^2}, \qquad (11)$$

where C is the solar constant and R_{ms} is the moon-sun distance measured in astronomical units. Similarly, the irradiance of the earthlight would be

$$I_e = \frac{C}{R_{es}^2} p_e f_e(\beta) \frac{R_e^2}{R_{em}^2}, \qquad (12)$$

where R_{em} and R_{es} are the earth-moon and earth-sun distances, respectively. Thus, the earth's reflectivity can be expressed as

$$p_e f_e(\beta) = \frac{I_e}{I_s}[\frac{R_{em}}{R_e}]^2[\frac{R_{es}}{R_{ms}}]^2. \quad (13)$$

In the observations, we study pairs of diametrically opposite fiducial patches, five in the earthshine and the other five in the sunlit part of the moon, both near the nighttime lunar limb. Hereafter when referring to radiances, we will use the term 'earthshine' to refer to the radiances measured for the five fiducial patches on the earthshine side of the moon, and we will use the term 'moonshine' to refer to the radiances measured for the fiducial patches located on the bright side of the moon bathed in sunlight. The term 'crescent' radiance will also be used in following sections, indicating the measured radiance averaged over the whole sunlit area of the moon.

For our purposes here, we call a representative pair of those opposing fiducial patches "a" and "b" and treat them as unit projected areas. If a is illuminated only by the earthshine, the radiance observed by an observer on the earth at a distance R_{oa} would be

$$I_a = I_e \frac{p_a f_a(\theta_0)}{R_{oa}^2} T_a, \quad (14)$$

where T_a is the transmission of the earthshine through the atmosphere, and $f_a(\theta_0)$ is the *lunar* phase function for the near retroflection from patch a, see Figure 1. Thus, I_a/T_a is the observed radiance corrected for airmass. Similar to Equation (14), the radiance of the sunlit portion, b, would be

$$I_b = I_s \frac{p_b f_b(\theta)}{R_{ob}^2} T_b, \quad (15)$$

where θ is the lunar phase angle and θ, like α and β, varies between 0 and $\pm\pi$, and where the lunar phase function, $f_b(\theta)$ embodies the dependence of the fiducial patch on the angle between the sunshine and the moonshine, see Figure (1). Thus,

$$\frac{I_a/T_a}{I_b/T_b} = \frac{I_e}{I_s} \frac{p_a f_a(\theta_0)}{p_b f_b(\theta)} \frac{R_{ob}^2}{R_{oa}^2}, \quad (16)$$

and so

$$p_e f_e(\beta) = \frac{I_a/T_a}{I_b/T_b} \frac{p_b f_b(\theta)}{p_a f_a(\theta_0)} [\frac{R_{es}}{R_e}]^2 [\frac{R_{oa}}{R_{ob}}]^2 [\frac{R_{em}}{R_{ms}}]^2. \quad (17)$$

Since $\frac{I_e}{I_s}$ is independent of lunar phase, Equation (17) is also independent of lunar reflectance provided all quantities labelled by "a" are derived from the earthshine, and all labelled "b" come from moonshine. However, we ultimately take p_a and $f_a(\theta_0)$ from moonshine data, which introduces a dependence on the lunar reflectance. This small effect (the effect of 50 Å shift in the spectrum is small compared to the spread among the $\frac{p_b}{p_a}$), and we treat it as being subsumed into that ratio, see section 4.4. Also, $[\frac{R_{0a}}{R_{0b}}]^2$ is so close to unity that we can safely set that factor in Equation (17) to unity. Thus, we determine that

$$p_e f_e(\beta) = \frac{I_a/T_a}{I_b/T_b} \frac{p_b f_b(\theta)}{p_a f_a(\theta_0)} [\frac{R_{em}}{R_e}]^2 [\frac{R_{es}}{R_{ms}}]^2. \quad (18)$$

We measure I_a and I_b in our nightly observations, and correct for airmass (e.g., I_a/T_a). We have measured the lunar phase function quite accurately over the last three years. We use total eclipse data from 93November 29 to measure the ratio of the geometrical cross-sections of the two fiducial patches, $\frac{p_b}{p_a}$. For our fiducial regions, this ratio ranges between 0.9 and 1.1. In section 5, we combine Equations (10) and (18) to define our measure of the earth's reflectivity, A^*, in terms of measured quantities, including the varying earth-moon distance.

3. Data Reduction

3.1. Image Analysis

The earthshine and moonshine (sunlit part of the moon) intensities are measured by integrating the brightness of a pair of fiducial patches – one from the bright side and the other from the dark side of the lunar disk. In our study, ten physically fixed fiducial patches have been used with

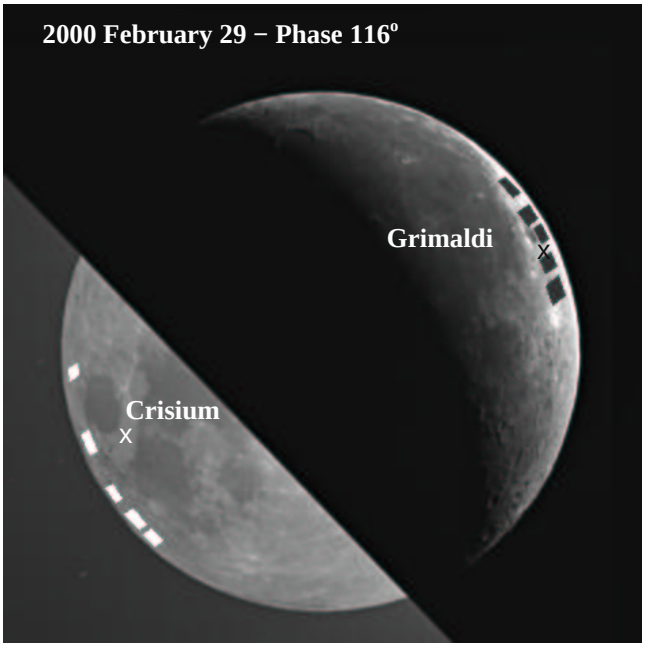

Figure 2. The moon showing the bright side and the earthshine. The Grimaldi side is in the moonshine and the Crisium side is in the earthshine. Our ten fiducial patches used in the observations made from BBSO are indicated. The crosses give the approximate positions of Danjon's fiducial patches. Goode et al. (2001) used one fiducial patch on each side, and on the Crisium side it is the one closest to the white cross, while on the Grimaldi side, it is the one immediately above the black cross. In the image, the lunar phase is 115°.9, near a declining quarter moon. Unlike the moonshine, the earthshine is flat across the disk. The flatness is due to the uniform, incoherent back-scattering (non-Lambertian) in contrast to the forward scattering of sunlight occuring in the sunlit lunar crescent surface.

five in the earthshine and five in the moonshine, see Figure 2. In selenographic (lunar) coordinates, the center latitudes and longitudes of the five patches on the Crisium side are (-17.5, -70.), (-11.2, -71.5), (-5., -76.), (0., -75.), and (7.5, -76.5), and those of the five patches on the Grimaldi side are (28.5, 72.5), (12.5, 75), (0., 77.), (-7.5, 75.), and (-13., 75.). Each patch covers a longitudinal range of about 10 degrees and latitudinal range of 3 to 5 degrees, the surface area being about 0.1% of the lunar surface, which corresponds to about 100 camera pixels. These patches are located in the "highlands" of the lunar surface, and the physical reflectivity of each is roughly comparable. One of the patches on the Grimaldi side is very close to Danjon's choice, while the patches on the Crisium side are all closer to the limb than Danjon's patch (Figure 2).

To locate these patches in each lunar disk image taken every night, it is essential to establish the transformation between the CCD image coordinate system and the selenographic coordinate system. For this purpose, we first define the limb and center of the lunar disk for each image. Each of the raw lunar images is contrast-enhanced, and the limb points are defined by looking for suitable positions of large intensity gradient. Empirically, a minimum of 40 rim points need to be obtained, and are then used to make a fitting to decide the lunar center in the image plane. Once the lunar center and limb are determined, the radius of the lunar disk is calculated in the CCD's coordinate frame. The next step is to define the position of the lunar pole in the image plane. To this end, some outstanding lunar features, whose precise selenographic coordinates are known, are used to co-register the two coordinate systems. The topocentric location of the lunar pole at any given moment can be precisely calculated using parameters from an astronomical almanac, from which one can determine the projected positions of these lunar features in the image plane, which is perpendicular to the vector pointing from the local observer to the lunar center. By comparing these projected positions with the positions of these features in CCD coordinates, the angle between the projected N-S axis of the moon and the Y-axis of the CCD coordinate system is derived. All our data reduction is done automatically by a software package specially developed for this purpose.

Once the transformation between the image plane and the selenographic system is established, the five pairs of fiducial patches can be precisely located on the lunar disk image. The apparent areas of these patches change from night to night because of lunar libration. The intensity is read out as an average of the whole area, and the difference due to the geometric effect of the reflectivity arising from libration is accounted for in our next step of data reduction (section 3.2).

To ensure accurate photometry, flatfielding and dark current subtraction are performed on each image. For earthshine images, we also need to subtract the background scattering from the bright side of the moon. The background scattering should be a function of both the inclination of the vector connecting the lunar center and the background point with respect to the lunar equator, and the distance from the background point to the crescent. After experimentation, we found that we could safely assume that on the earthshine side, where the background points are not too close to the crescent, at a fixed inclination with respect to the lunar equator, the background intensity falls off linearly with the distance of the background point to the lunar center. Such a linear relation holds for the points that are not too far from the lunar equator. So, for each fiducial patch centered on the vector connecting the lunar center and the patch, we open a small cone with an angular size 5°, and fit the intensities of the background points, which are beyond the lunar limb and inside the cone, as a function of their distance to the lunar center. In this way, we can extrapolate the scattering intensity to the position of the fiducial patch using the parameters obtained from the least-square fit, and then subtracting the linearly extrapolated value from the intensity of the fiducial patch. This procedure is illustrated in Figure 3.

In accordance with Equation (18), the intensity obtained from above is also corrected by scaling to a set of standard distances between the sun, moon and earth, before the successive steps of calibration described in subsequent subsections. Precise distance parameters are obtained from an ephemeris.

3.2. Atmospheric Extinction

To eliminate the effect of the atmospheric extinction, observations are carried out for as long as possible during the night, so that a measurement of the intensity at varying airmass can be obtained. For the bright side of the moon, we expect the variation of the intensity to follow Beer's law:

$$I = I_0 e^{(-\alpha\eta)}, \tag{19}$$

where I is the observed intensity, α is the atmospheric extinction coefficient, η is the local airmass and I_0 is the intensity at zero airmass – the intensity if the earth had no atmosphere.

The airmass, η, is determined from the angular altitude of the moon in the sky at different times in such a way that when θ_c - the zenith angle of the ground observer's view of the moon, which is the complement of the moon's angular altitude - is smaller than 60°, $\eta = 1./\cos(\theta_c)$; otherwise η is interpolated from a standard airmass table (Table 1).

The above calculation refers to the airmass at sea level with the pressure $p_0 = 760$ mmHg and temperature $t_0 = 10^\circ C$, and the real airmass at the observer's location must be

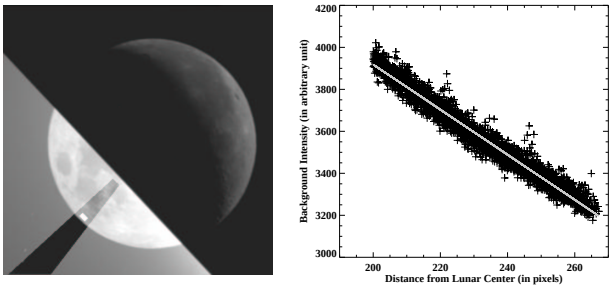

Figure 3. Illustration of the background subtraction for earthshine images. The image on the left shows a background cone around a fiducial patch, within which the intensity of the background points are read out to make a fit as a linear function of the distance from the lunar center. For the image shown, the intensity inside the cone has the background subtracted already. The plot on the right shows the decline of the off-limb intensity as the background point gets further from the lunar center, and the overplotted thick grey line indicates the least-square linear fit.

Table 1. Standard Airmass Table (θ_c in degrees)

θ_c	60.	62.	64.	66.	68.	70.	72.	74.	76.	78.	80.
η	2.00	2.12	2.27	2.45	2.65	2.90	3.21	3.59	4.07	4.72	5.60
θ_c	81.	82.	83.	84.	85.	86.	87.	88.	89.	90.	-
η	6.18	6.88	7.77	8.90	10.39	12.44	15.36	19.79	26.96	40.00	-

corrected by a multiplicative factor of $p/p_0/(0.962+0.0038t)$ (Allen, 1973). BBSO is 2067m above sea level, and the pressure scale height at this altitude is 8200m, which yields $p = p_0 \exp(-2067./8200.)$. We then incorporate the calculated η into the Beer's law fitting to determine α and I_0. We reckon that throughout a night, the evolving lunar phase function can also contribute to the changing intensity. The maximum phase change in a long night is less than two degrees, within which the intensity change is negligible compared to the change due to the airmass. Nevertheless, we employ a quasi-iterative way to correct this minor effect, in that we use an initial fit of the phase function to correct the data, and after the airmass correction, we make the phase function fit again. See the following section on how to obtain the phase function. After a few iterations, the data converge to a stable result. The observed intensity at each moment, I_i, is corrected, using the airmass, to the intensity at zero

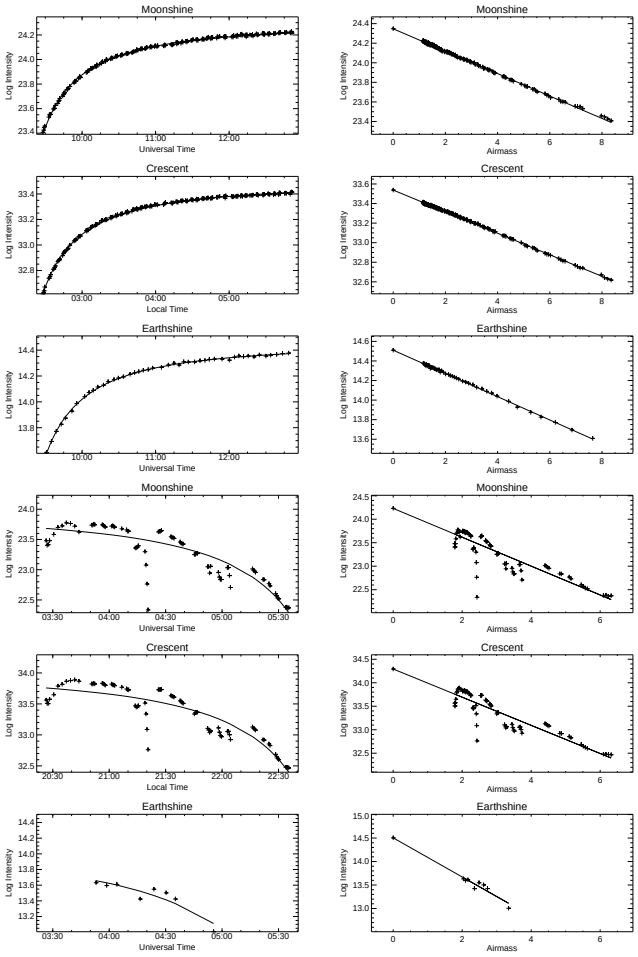

Figure 4. In each of the four tryptics of the figure the intensity per unit (lunar) area of the moonshine (top panel), the crescent (middle panel), or the earthshine (bottom panel), is plotted against time (on the left) and airmass (on the right). These intensities are data count values read from the CCD, corrected for all the steps indicated in section 3.1, and divided by the lunar phase function. In the case of moonshine and crescent intensities, the value has been also divided by the transmission of the bright side filter. The "+"'s indicate observed data points, and the solid lines are the fits to Beer's law. *Upper six panels:* data from the night of September 5, 1999, demonstrating a typical good night, and the standard deviation of the fitting is 0.007, 0.005, 0.007 (from top to bottom). *Lower six panels:* data from the night of September 17, 1999, demonstrating a typical, partly cloudy night, and the standard deviation of the fitting is 0.219, 0.183, 0.077 (from top to bottom).

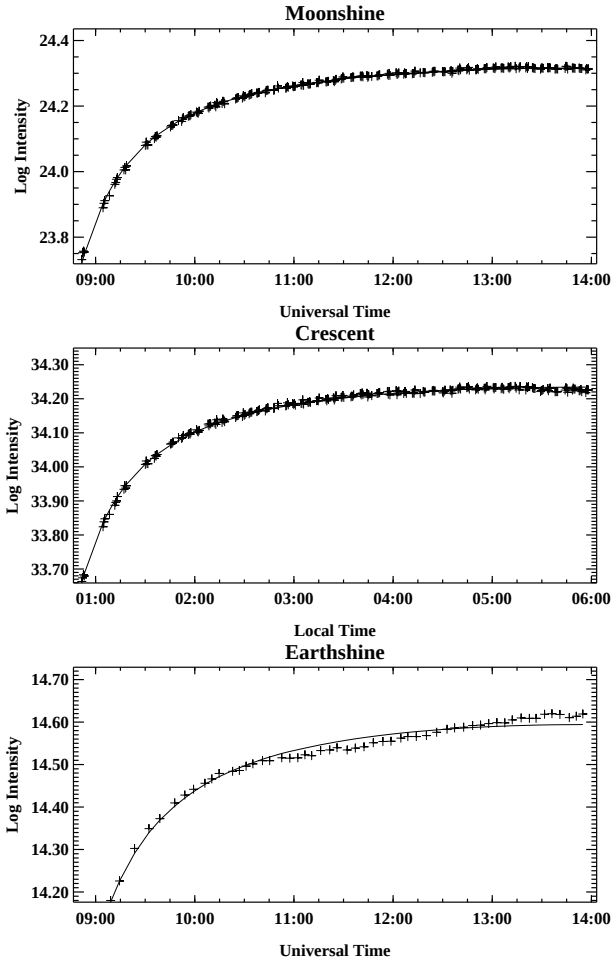

Figure 5. The moonshine, crescent and earthshine intensities and their Beer's law fit for the night of 2000 January 28, showing that while the moonshine and crescent intensities follow Beer's law very well, the earthshine intensity evolution deviates from Beer's law. The standard deviations of the fits are 0.004, 0.005, 0.014, respectively. The fact that the fit is poor only for the earthshine implies sizeable short-term variations in the earth's effective albedo as seen from BBSO due to a combination of factors including, among others, the earth's rotation, anisotropic reflectance and weather changes.

airmass, $I_i^0 = I_i \exp(\alpha\eta)$. I_0 from the fitting is further used as the intensity for that night's lunar phase function.

The goodness of the fit to Beer's law offers a ready criterion by which each night's local sky can be judged – the "good" night's data can be separated from that of the "bad" (noisy) night's (Figure 4). In practice, unless it is cloudy, the data from almost all observable nights are preserved, and the standard error in the fitting for each night is further used as the input error for the lunar phase function fit. Figure 4 shows an example of a typical good night and bad night, as judged by fitting to Beer's law. Experience from the observations shows that the data usually follow Beer's law quite well, and the accuracy of the moonshine fitting is often better than 1%. Among all the datasets collected for 340 nights from November 28, 1998 to March 31, 2002, the accuracy of the fitting is better than 1% for 110 nights, and the accuracy is between 1% and 2% for 139 nights, and between 2% and 3% for 52 nights.

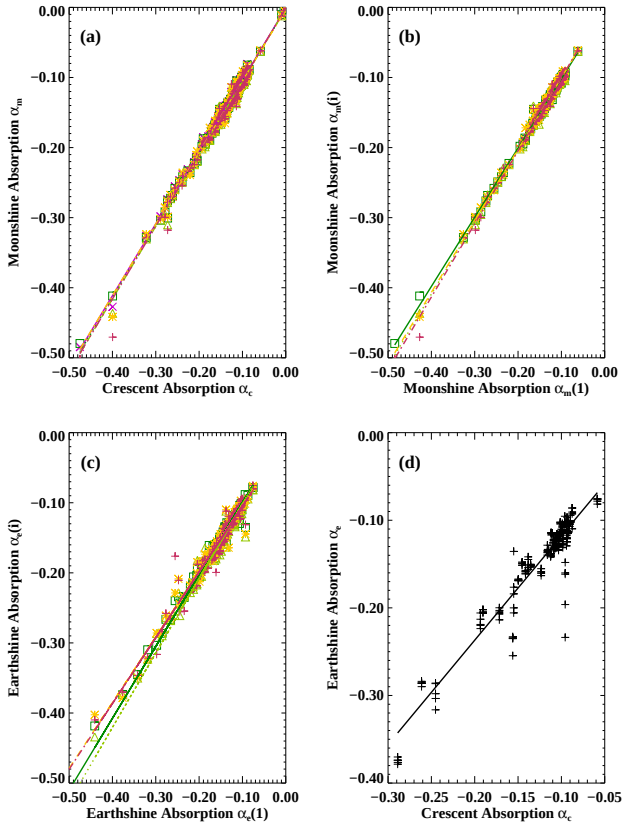

Figure 6. The variation of the atmospheric extinction coefficients for the crescent, (α_c), moonshine (α_m) and earthshine (α_e). Panel (a) illustrates α_m (for five fiducial patches as indicated by different symbols) against α_c from which it is clear that the crescent and moonshine patches are very much alike; (b) shows α_m of four out of five fiducial patches (as indicated by different symbols) vs. the fifth fiducial patch, illustrating that α_m is virtually the same for different patches (note the equivalence of each linear, least squares fits to the data for each patch); (c) shows α_e for four out of five fiducial patches (as indicated by different symbols) vs. the other fiducial patch, showing that α_e is also the same for different fiducial patches in the earthshine; and (d) shows α_e (of all fiducial patches in earthshine) against α_c, which is consistent with the earthshine being bluer than the moonshine. The various straight lines in each panel indicate a least squares fit to the appropriate data.

In the case of earthshine intensity, apart from the atmospheric transmission, the evolution of the earthshine is also influenced by changing of the earth during a given night; e.g., the sun rising over a cloudy China. In addition, almost every month, on a few nights, we observe that the evolution pattern of the earthshine intensity does not track Beer's law in an unambiguous way, even though the moonshine intensity closely follows Beer's law. An example of such a case is shown in Figure 5. In general, the fit to the earthshine yields a standard deviation that is larger than that for the moonshine fitting by one-half to one percent. This latter difference contains the signal of the earth's albedo variations. On such nights when the evolution of the earthshine is significantly controlled by real changes in the earth's reflectance, apart from the atmospheric extinction, as illustrated in Figure 5c, the atmospheric absorption coefficient α obtained from the Beer's law fitting of the earthshine observations may deviate from the true value. That is, some part of the earthshine signal may be subsumed into the atmospheric extinction, and vice versa, so that the correct atmospheric attenuation cannot be properly determined from the standard Beer's law fitting.

To deal with this problem, we investigated the relationship between the atmospheric absorption coefficients for radiances measured at the five patches on the earthshine side of the moon ($\alpha_e^i; i = 1, 2, 3, 4, 5$), the radiance of the five patches on the bright side or moonshine (α_m^i) and the radiance of the total area of the crescent (α_c). Figure 6 (a) and (b) show the relationship between α_c and the α_m^i for all five fiducial patches. Least-square fits reveal that the α_m^i ($i = 1, 2, 3, 4, 5$) can be regarded as being identical to one another, and to α_c. This is not a surprise, even though the atmospheric attenuation is also a function of the wavelength, as the light from a moonshine fiducial patch should have the same spectrum as the light from the whole bright side. Similarly, the earthshine absorption coefficient, α_e, is linearly correlated with α_c (Figure 6 (d)), but the absolute value of α_e is systematically larger than that of α_c, indicating a stronger atmospheric attenuation in earthshine than in moonshine. This is because the earthshine and the moonshine have different spectra, specifically, the earthshine is bluer than the moonshine (Tikhoff, 1971; Arnold et al, 2002; Woolf et al, 2002), because the bluer the light the more effectively the earth's atmosphere scatters it away by Rayleigh scattering.

The solution to fitting nights like those shown in Figure 5 lies in exploiting the linear scaling law that we find between α_e and α_c. This scaling enables us to make a better determination of α_e from α_c for the nights when the usual, local airmass changes leading to a good Beer's law fit for the moonshine, are compounded by sharp earthshine variations. In those cases, the mixture yields observational earthshine

Table 2. The coefficients α_e against α_c

q	a	b	σ	σ_a	σ_b
1.0	1.1886	-0.0073	0.0099	0.0183	0.0023
1.2	1.1830	-0.0061	0.0128	0.0170	0.0023
1.5	1.1813	-0.0051	0.0132	0.0172	0.0023
1.8	1.1881	-0.0050	0.0140	0.0171	0.0023
2.0	1.2281	-0.0095	0.0167	0.0169	0.0023
2.5	1.2222	-0.0124	0.0164	0.0161	0.0022

data that deviate sufficiently from Beer's law, so that one cannot be confident of the fit obtained in the usual way. Our solution lies in using α_c to fix α_e for the problematic nights, beginning with

$$\alpha_e = a \times \alpha_c + b, \tag{20}$$

where the scaling parameters a and b are obtained by a linear least-square fit of the above relation using α_e and α_c from the nights that do not show apparent global evolution that strays strongly from the Beer's law fit. We reckon that for the nights of significant global change, the standard deviation of the Beer's law fitting of the earthshine (σ_e) must be a lot larger than that of the crescent (σ_c), given that the local atmosphere is reasonably stable throughout a single night. For this reason, we make a further assumption that when σ_e is less than a cutoff value q times σ_c, i.e., $\sigma_e < q\sigma_c$, we regard the global change as not being significant during this night, and α_e from the Beer's fitting for this night is reliable. Only then do we use these nights to make the fit in order to determine a and b.

In Table 2, we list the fitting results, a, b, σ (the standard deviation of the fit), σ_a and σ_b (the fitting errors of a and b respectively) for various cutoff values, $q = 1.0, 1.2, 1.5, 2.0, 2.5$.

We can see from Table 2 that for $q < 2.0$, the fitting results are consistent with each other. In general, the absolute value of α_e is larger than that of α_c by more than 0.01, or about 10%. That is, using $\alpha_c \sim 0.1$ and Table 2, we have $\alpha_e \sim 1.2 \times \alpha_c - 0.01 \sim 0.11$. We first tried to scale α_e^i to α_c separately, and the resulting fitting parameters a and b did not differ for different patches. Thus, we do not distinguish among the α_e from different fiducial patches, because there is no reason for us to believe that the α_e^i should be different from one another (also see Figure 6c). In the subsequent analysis, we employ the scaling parameters at $q = 1.2$ in Equation (20) to obtain α_e from α_c for nights when $\sigma_e > 1.2\sigma_c$. Then, we use α_e to fit out the atmospheric attenuation, so that we can determine the true earthshine signal. After applying this correction, a direct result is that while the average of the A* is not altered, for some nights their appreciable, original deviations from the average, at comparable lunar phase, is greatly reduced. For those same nights the calculated α_e yields a slightly poorer fit to the data than would a direct fitting to Beer's law. The price of this latter fitting was to force some of the earthshine signal into the atmospheric extinction coefficient, yielding an erroneous extrapolation to zero airmass.

4. The Lunar Phase Function

The lunar phase function is defined as the normalized change in the moonshine intensity as a function of lunar phase, which represents the geometric reflectance of the moon. It is measured from the readout intensity of each of the fixed fiducial patches (five on the Crisium side and five on the Grimaldi side) used throughout the observations, after carrying out several straightforward corrections to the raw data. When the observed intensity readout is plotted against the lunar phase for all nights, the data are quite scattered around different means for each branch, as illustrated in Figure 7, for the Crisium and Grimaldi pair used in Goode et al. (2001). This figure, and that pair, are treated in detail in this section. The raw results for all pairs take the same form as the chosen pair that is used for Figure 7. On the face of it, the large scattering of data in Figure 7 would seem to preclude a precise determination of the earth's albedo from measuring the earthshine. However, most of the scattering of data is due to known physical effects for which one can systematically account, and then remove.

The first factor is the night-to-night change of the local atmosphere, apart from the nightly atmosphere attenuation which follows Beer's law. Such a change affects the measured crescent as a whole, and moonshine and earthshine from the fiducial patches in precisely the same way, and hence, the raw phase function can be corrected by treating the crescent as a standard star (see section 4.1). This correction does not alter the determination of A^*, because the correction applies to both the earthshine and moonshine, while A^* is given by the ratio of the earthshine to the moonshine. The second factor is the sun's position, namely the declination and right ascension, due to the changing angle of the sunlight into the earth-moon system at the same lunar phase, but in different synodic months. This changes the range of well-illuminated latitudes both on earth and the moon from one month to the other. To first order, we fit out the alteration of the scattering introduced into the phase function. (see section 4.2). Since it affects the moonshine and earthshine intensities in the same way, again A^* is insensitive to the change. The third known source of the scatter in Figure 7 is the moon's libration, which changes the observed intensity from the moonshine fiducial patches, but does not affect the earthshine intensity (see Figure 2 in which the non-uniformity of the moonshine near the limb is apparent, but there is no such non-uniformity in the earthshine). To first order, we model this effect as a linear function of the libration and correct it for both the phase function and in the moonshine intensity I_b, when using I_b to calculate A^* (section 4.3). The results of these corrections are developed in this section, one step at a time. We shall see that we can determine the lunar phase function to 0.5%, which gives us real confidence that observing the earthshine can yield a precise reflectance for the earth.

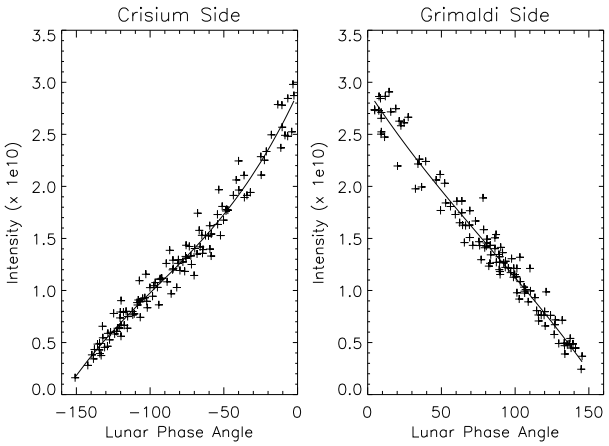

Figure 7. The intensity of the *moonshine* for the Crisium side and Grimaldi side fiducial patches of Goode et al. (2001) with a third order polynomial (including higher order terms has no noticeable effect) fit for each. Clearly, there is a roughly linear decrease in the intensity of the reflected light going from full moon to new moon.

In the last part of this section (4.4), we normalize the overall lunar phase function to connect the right and left branches of the lunar phase function by treating the opposition surge that occurs at small phase angles (Hapke, 1971; Flatte et al, 1991; Helfenstein et al, 1997). The data here are from the fullest of full moons and the one total lunar eclipse we observed in Big Bear. The total eclipse enables us to determine the ratio of the geometrical albedos of the opposing pairs of fiducial patches.

4.1. Atmospheric Correction

The nightly fits of the moonshine intensity to Beer's law are quite good, and so the extrapolation to zero airmass would seem quite reliable. However, there is an appreciable change in our lunar phase function (see Figure 7), for the same phase, from month-to-month. As we shall see, the prime cause of this is that, even after extrapolation to zero airmass, the resultant intensity is subject to changes in the local atmospheric conditions. It seems that the local atmosphere is not a uniform plane, parallel gas, but rather we have something more like a canopy superposed on a plane parallel atmosphere. The canopy mutes the intensity by the same amount for all airmasses, and therefore its effect remains after extrapolation. Because of this, there is a deviation in the intensity measured from the same fiducial patch at the same lunar phase, but on different nights (that is, successive lunar cycles). To solve this problem, we employed the common practice of nighttime observers; when doing absolute photometry they use standard stars to account for the muting. We have found that the crescent of the moon (the total area illuminated by sunlight) is our best standard "star". That is, we correct from night-to-night variations using the correlation between the change of the moonshine intensity and the crescent intensity.

In the extrapolation to zero airmass, we use a fifth degree weighted polynomial fit for both the fiducial patch intensity and the average crescent intensity over the area of the bright portion as the way to determine the average of the intensity at each lunar phase. In removing the canopy effect, we give double weight to nights for which the lunar phase is less than $\pm 5^\circ$. We do this because of the pronounced opposition effect that gives a sharp increase in the moonshine intensity when lunar phase approaches zero degrees (see §5.4). The deviation of the measured intensity at each data point from the fitting curve for the lunar phase function, in both the moonshine case and the crescent case are obtained, and the cross correlation between these deviations is calculated. For the morning observations, for which the lunar phase is positive, we get a cross correlation of 0.73, and for the evening when the lunar phase is negative, we obtain a quite similar value of 0.77 (Figure 8). The relative correlations are determined from a simple least-square linear fit between the moonshine deviation and crescent deviation using

$$\frac{I_i - \bar{I}_i}{\bar{I}_i} = a_0 \times \frac{C_i - \bar{C}_i}{\bar{C}_i} + b_0 + \sigma_i, \qquad (21)$$

where I_i is the observed fiducial patch intensity, C_i is the crescent intensity, $\bar{I}_i$ and $\bar{C}_i$ are the average fiducial patch intensity and crescent intensity, respectively, at the same lunar phase, and σ_i is the scatter about the linear least-squares fit. Note that throughout this section $\bar{I}_i$ is the final, fitted intensity, which is derived by iterating the steps described in sections 4.1-4.3. The coefficients a_0 and b_0 are derived from the least square fitting of Equation (21). From Figure 8, it is clear that a_0 is close to unity (morning/Grimali:0.81±0.08 and evening/Crisium:0.74±0.07, error is $\pm 1\sigma$), while the respective b_0's are essentially zero – 0.002 and 0.001 – more than two orders of magnitude smaller than a_0. Therefore, we determine the correct, relative zero airmass intensity, I'_i, by removing the canopy effect by subtracting the linear term in Equation (21) from the earthshine data, i.e.,

$$I'_i = I_i - a_0 \times \bar{I}_i \times \frac{C_i - \bar{C}_i}{\bar{C}_i}. \qquad (22)$$

The scattering among the datapoints is much reduced after this correction (see Figure 11b at the end of the section). This correction is of comparable significance for the evening data (lunar phase < 0) and the morning data (lunar phase > 0), as the comparable cross-correlations imply.

4.2. Declination Correction

The second step in correcting the deficiencies in the apparent lunar phase function is to remove variations arising from the systematic change of relative position of the moon to the plane of the earth's orbit about the sun. The difference in right ascension between the sun and the moon (hereafter, the "relative right ascension") changes from 180 to -180°, which essentially determines the lunar phase, defined as the angle from between the moon-earth line and the sun-moon line, see Figure 1. However, there is an ambiguity in the lunar phase angle that makes the apparent lunar phase function multi-valued. In detail, the difference in the declination between the sun and the moon (hereafter "relative declination") changes as well, since the orbital plane of the moon around earth is inclined to that of the earth around the sun. Toward the full moon, the relative declination also becomes important in determining the lunar phase. Then, at the same lunar phase, but on different nights (that is, different months), the position of the moon may be different, and this difference alters the readout intensity of the fiducial patches. To correct for this effect, for a given lunar phase near the full moon, we choose a standard position of the moon and normalize the readout intensity of different positions to this standard position. The standard position is the one for which the relative declination is zero, i.e., the moon is in the plane of ecliptic, and the lunar phase is equal

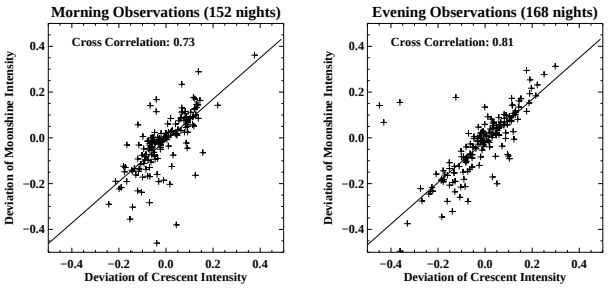

Figure 8. The deviation of the moonshine fiducial patch intensity from average against the deviation of the overall intensity of the crescent. Left: data points from morning observations of Grimaldi; right: data points from evening observations of Crisium. The solid lines in each panel show the linear fit to each cluster of points.

to the relative right ascension, i.e., a total lunar eclipse. The normalization is made as follows:

$$I_i - \bar{I}_i = a_1(P_i - P_{i,RA}) + b_1 D_i + c_1 + \sigma_i, \qquad (23)$$

where I_i is the observed intensity, $\bar{I}_i$ is the average intensity at the same lunar phase as I_i (from the ultimately determined lunar phase function), $(P_i - P_{i,RA})$ is the difference between the lunar phase and the relative right ascension, D_i is the relative declination, and a_1, b_1, and c_1 are fitting parameters, which are determined from the least-square fitting using all the observed intensities. The fitted parameters, a_1 (morning/Grimaldi: -0.003 ± 0.002 and evening/Crisium: $3.4e^{-5} \pm 7.0e-5$), b_1 (morning/Grimaldi: $-0.4.7e^{-5} \pm 0.0002$ and evening/Crisium: 0.0007 ± 0.0002) and c_1 (morning/Grimaldi: 0.009 ± 0.008 and evening/Crisium: 0.009 ± 0.009) are all quite small. All quoted errors are $\pm 1\sigma$. The normalized intensity, I'_i, is derived by removing the relative right ascension and declination:

$$I'_i = I_i - [a_1(P_i - P_{i,RA}) + b_1 D_i]. \qquad (24)$$

The c_1 term is regarded as part of the errors (σ_i).

This correction is only made for lunar phase between -15 and +15 degrees since the effect of the relative position of the moon is only important around the full moon. However, the modest improvement due to this correction reveals barely apparent changes in the data points.

4.3. Libration Correction

The third step in rectifying the apparent lunar phase function requires removing the effects of latitudinal and longitudinal lunar libration. Since the orbit of the moon around the earth is not in the equatorial plane of the earth, a terrestrial observer alternatively sees the north pole and south pole of the moon during each orbit. This is the latitudinal libration. Further, the slightly elliptical orbit of the moon has the consequence that the moon moves more slowly at apogee than at perigee, and therefore is seen to be wobbling around its axis of rotation. This is longitudinal libration. An additional, very small dynamical libration arises because the moon is prolate, and its pointing wanders. The dynamical libration adds to both the latitudinal and longitudinal librations. These librations allow us to see about 60% of the moon's surface. As a result of both kinds of libration, for different cycles of the lunar orbit, even at the same lunar phase, we would expect changes in the positions of the fiducial patches on the lunar disk. The readout intensity thus changes as a function of the geometric position of the fiducial patches on the lunar disk. The longitudinal and latitudinal librations cause the apparent lunar phase function to be multi-valued. To first order, we derived a description of the deviation of the observed intensity from the averaged intensity as a linear function of the longitudinal and latitudinal librations, which goes as:

$$I_i - \bar{I}_i = a_2 L_i^{\alpha} + b_2 L_i^{\beta} + c_2 + \sigma_i, \qquad (25)$$

where the $I_i - \bar{I}_i$ are the deviations of each night from the mean, and where L_i^{α} is the longitudinal libration and L_i^{β} is the latitudinal libration. Here, L_i^{α} and L_i^{β} really measure the position of the lunar pole in the sky with respect to its mean position, so that all the kinds of libration are taken into account. From a least-squares fit, we obtain the coefficients a_2 (morning/Grimaldi: 0.0019 ± 0.0004 and evening/Crisium: -0.0018 ± 0.0004) and b_2 (morning/Grimaldi: $4.2e-5 \pm 0.0003$ and evening/Crisium: -0.0003 ± 0.0004), while c_2 is 1-2 orders of magnitude smaller than a_2. Again all quoted errors are $\pm 1\sigma$. Since the magnitude of the a_2's are about an order of magnitude greater than the b_2's, the longitudinal libration is more significant than the latitudinal libration. Figure 9 shows the result of fit, and, in particular, that the fit describes the data, in that it can be seen that the observed scattering at this step is mainly accounted for by the libration. For the determination of Figure 9, we used 152 mornings and 168 evenings, and the correlation between the fit and the data is 0.44/0.52 respectively. Using the parameters from the fit, we then normalize the intensities at all lunar phases to the case of zero libration with the equation:

$$I'_i = I_i - (a_2 L_i^{\alpha} + b_2 L_i^{\beta}). \qquad (26)$$

To check the validity of the libration correction, we performed the libration correction again – but doing it before performing the atmospheric correction described in §5.1. We next performed the atmospheric correction (which still dominates) and the declination correction. At that point, we performed the libration correction again, and we found that $I_i - \bar{I}_i$ does not have a significant correlation with the libration. In particular, the parameters from the linear fit of Equation (25) are reduced by an order of magnitude. This test not only confirms the validity of the libration correction performed above, but also guarantees that the three-step corrections can be performed in any order. However, it remains for us to determine the lunar phase function for small phase angles.

4.4. Opposition Effect

To this point, the lunar phase function is incomplete because it is not normalized, and we have not determined its functional form for the smallest phase angles. To do these, we need to know the phase function for small phase angles, and that means that the final lunar phase function for each fiducial patch needs to be normalized to the full moon opposition peak. In reality, the moon is not observable at zero lunar phase because the shadow of the earth would occult

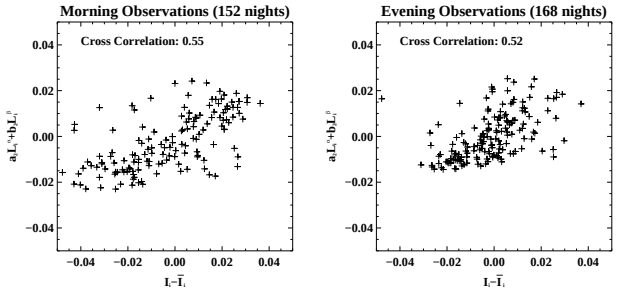

Figure 9. The deviation of the moonshine fiducial patch intensity (after the first and second step corrections) from average against the deviation as a fitting result from Equation (25). Left: data points from morning observations; right: data points from evening observations.

the moon, as the earth's shadow occupies about $\pm 0.8^\circ$. So far, the smallest phase we have reached is $\pm 1.0^\circ$ on the night of November 29, 1993, when a total lunar eclipse occurred over Big Bear. On that night, the sky was clear and stable throughout, and observations were made both before and after the total eclipse, covering lunar phase angles of magnitude ranging between about 1° and 2°, which offers a unique dataset to investigate the slope of the opposition surge effect for all fiducial patches on both the Grimaldi and the Crisium sides.

The images taken during the eclipse were processed, and the intensities of the fiducial patches were read out as described in Section 4.1. The atmospheric attenuation has to be corrected to obtain the real moonshine intensity. However, throughout the night, the evolution of the moonshine intensity was controlled not solely by the changing airmass, but also by the changing phase angle. This latter effect is appreciable because of the strong opposition effect at small lunar phase angles. As a result, the shape of the intensity evolution for the two patches deviates strongly, compared to the precision in the data, from Beer's law (see Figure 10a and c). Thus, Equation (19) can no longer produce a reasonable fit.

We developed a simple solution to this problem under the reasonable assumption that the opposition effect is linear for very small phase angles, say, from 0 to 5° (Hapke, 1971 and 1998). During the eclipse, the phase angle changes by less than two degrees for either the Crisium branch or the Grimaldi branch. To determine the slope of the opposition peak for each of the ten fiducial patches, we represent the observed intensity by:

$$I_i = I_0 \times (1 - \gamma |P_i|) \times e^{-\alpha \eta_i}, \qquad (27)$$

where I_i is the observed intensity at phase angle $|P_i|$ (in degrees) and airmass η_i. In contrast to Equation (19), I_0 describes the intensity at both zero airmass and zero phase angle. The second term on the right side describes the linear increase of the phase function as the lunar phase goes to zero. The last term describes the exponential atmospheric attenuation; i.e., Beer's law, where α is the atmospheric absorption coefficient for the moonshine.

In applying Equation (27), we used the observed I_i, after correcting for libration (section 4.3) at lunar phase P_i and airmass η_i in Equation (27) above, and made a least-squares, non-linear fit to obtain α, I_0, and the linear opposition effect coefficient, γ, and corrected for pennumbral shadowing for the very smallest phase angle data. The fit was made for all ten fiducial patches. We did not correct for the declination because the moon is in total eclipse, and that correction should be quite small. We collected about 40 data points for the fit on each side of the moon; i.e., before and after totality, and the standard deviation of the final fit is at the level of 0.5%. Figure 10b and d reveal the improvement in fitting results for one pair of fiducial patches using Equation (27) instead of Equation (19). The improvement is typical of that for all ten patches. From Figure 10, it is also clear that Equation (27) accurately describes the composite effect of the opposition surge and Beer's law. The fitted opposition peak slope parameter, γ, was then used to normalize the phase function for each of the fiducial patches. Figure 11 shows an example of the final lunar phase function normalized to the opposition peak. Of course, each fiducial patch has its own lunar phase function. In detail, for lunar phase of 5° in Figure 11, we used the slope, γ, determined for very small angles to extrapolate to the intensity at zero lunar phase from that at 5°, i.e., $I(0) = \frac{I(5)}{1-\gamma \times 5}$. Then, we normalized that branch of the phase function, using its γ and $I(0)$=1 to fix $I(5)$. Combining our knowledge of $I(5)$ with the relative phase function indicated by the +'s in Figure 11, we obtained the right branch of that figure. The normalization removes the ratio of the geometrical albedos between the two patches, which is restored in Equation (28). The eclipse does not give us data for lunar phase $2^\circ < |\theta| < 5^\circ$,

Table 3. Opposition Effect γ's, see Equation (27)

Patch	1	2	3	4	5
Grimaldi side	0.084	0.078	0.083	0.079	0.083
Crisium side	0.086	0.079	0.076	0.083	0.083

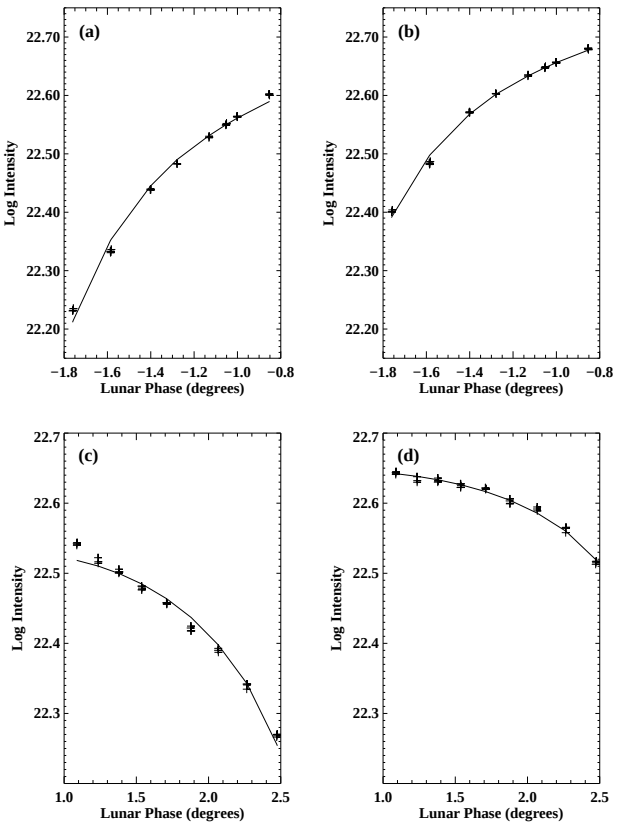

Figure 10. Fit of lunar eclipse data obtained on November 29, 1993. (a) Beer's law fit of the Crisium side (Equation 19); (b) Composite Beer's law plus opposition effect fit on the Crisium side (Equation 27); (c) same as (a) on the Grimaldi side; (d) same as (b) on the Grimaldi side.

Table 4. $\frac{p_a}{p_b}$ (Crisium Side/Grimaldi Side)

Patch	1	2	3	4	5
6	1.121	1.130	1.141	1.086	1.109
7	1.041	1.050	1.060	1.009	1.030
8	0.919	0.926	0.935	0.890	0.909
9	0.983	0.991	1.001	0.953	0.972
10	0.989	0.996	1.006	0.958	0.978

where we have also assumed a linear form for the phase function. Nights at these small phase angles occur at the fullest of full moons, and we have a few of them. We will enrich our data in this region as time goes on, and can further sharpen our phase function. If there were a systematic error here, it would shift all of our Bond albedos by the same amount. We expect such a systematic error is actually quite small, but we would be able to re-calibrate our present results in the light of future data.

In Table 3, we list the values of the derived opposition coefficients, γ, for all ten fiducial patches. The value of γ for all fiducial patches is approximately 0.08 per degree, indicating that when lunar phase changes from six degrees to zero degrees (full moon), the intensity doubles. This is the well-known opposition surge which had not been quantitatively determined previously. The formal error in the determination of γ is about 0.5%.

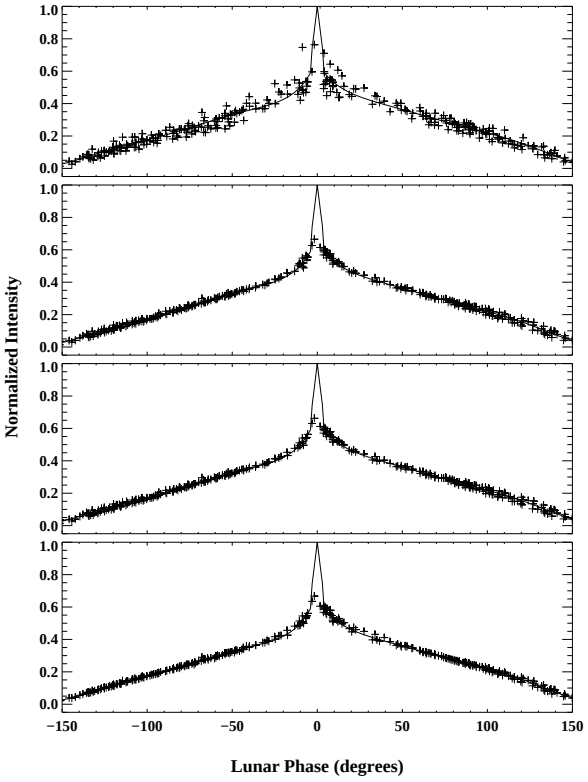

Figure 11. The top panel shows the apparent, relative lunar phase function from the raw data, for which there are points down to 2°. The function is made relative by normalizing it to unity at phase angle 0°, which means that the ratio of the true right and left branch intensities yields the ratio of the geometrical albedos between Crisium and Grimaldi. The peak near small phase angles represents the opposition effect. Data from a total eclipse are used to connect the positive and negative phase branches of the lunar phase function. No eclipse data are shown in this figure, but the result of the eclipse data is the opposition peak. The second panel from the top shows the result after including correction for the local atmospheric effects using the lunar crescent as a guide star. The third panel also includes the correction for lunar declination. The fourth panel includes the correction for lunar libration. The fit shown in each panel is the final one resulting from all of the corrections described in section 5.

The parameter I_0 is also used to obtain the ratio of the earthshine patch reflectivity to the moonshine patch reflectivity p_a/p_b. Table 4 gives the ratios determined between each of the five Crisium patch reflectivities to the each of Grimaldi patch reflectivities.

In Figure 11, we show the lunar phase function with final fit in the lowest panel. The same fit is shown in the other three panels, as well. The points in the top panel represent a normalized version of Figure 7. The second panel shows the result after correction for local atmospheric effects, which is the largest correction. The third and fourth panels show the effects of lunar declination and libration, respectively. The lunar phase function is produced from a fifth degree weighted polynomial fit to the corrected data. After each step of correction, the standard deviation of the fit is reduced from originally 0.05/0.05 (evening/morning) to eventually 0.01/0.01, with the phase function normalized to unity. A restricted regularized fitting is performed as well, which parameterizes the intensities at 181 bins (corresponding to lunar phase 0° to 180°).

These 181 parameters from the fitting describe the lunar phase function, in that the intensity of any lunar phase is the linear interpolation between the values at the two grids into which the lunar phase falls. Note that since there are no data points beyond 150° degrees, the phase function fit beyond this range is not reliable. Similarly, there are not enough data points within ±5°, and so, we used the eclipse data to determine the fitted peak in Figure 11 by treating opposition effect at small phase angles (near the full moon). From the final fit, the estimated error of the mean is at the level of 0.5%; thus, we have measured the lunar phase to 0.5%. How does the phase function in the lowest panel of Figure 11 compare with earlier efforts to determine it, like those of Danjon?

In Figure 12, we plot Danjon's fitted phase function against our corrected one. Danjon used slightly different fiducial patches, but that is not the source of differences, because the phase function shown is about the same for all

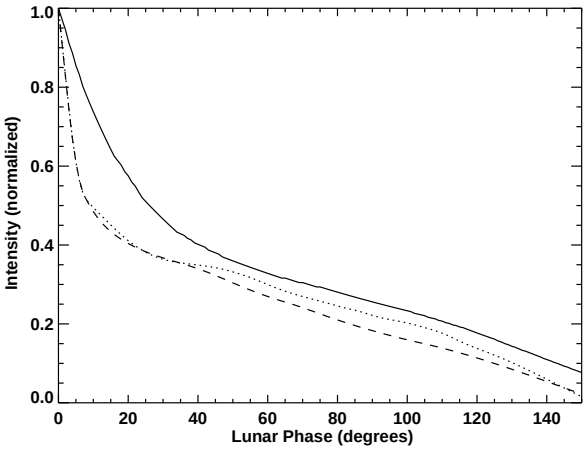

Figure 12. Danjon's phase function (solid line) is plotted against lunar phase. Using Figure 11d, the dashed line is our phase function for evening observations and the dotted line for morning for the fiducial patch of Figure 11.

of our fiducial patches. Rather, the primary source is the opposition surge which was unknown in Danjon's time. There is a clear offset in the Danjon phase function which would yield uniformly higher albedos than the true phase function. For our phase function, we have eliminated this erroneous overestimate, by ~20%, of the earth's reflectance introduced by the phase function in earlier incarnations of earthshine studies, like those of Danjon.

5. Precision of the Determination of the Earth's Nightly Albedo

The effective albedo for an individual night is calculated from the earthshine measurement for that night by combining equations (9) and (17):

$$A^*(\beta) = \frac{3}{2f_L}\frac{p_b f_b(\theta)}{p_a f_a(\theta_0)}\frac{I_a/T_a}{I_b/T_b}\frac{R_{em}^2}{R_e^2}\frac{R_{es}^2}{R_{ms}^2}, \qquad (28)$$

where $\frac{I_a/T_a}{I_b/T_b}$ is the ratio of the earthshine intensity to the moonshine intensity in two opposing fiducial patches, after correcting for airmass. The ratio between the physical reflectivity of the two opposing fiducial patches, $\frac{p_b}{p_a}$, is determined from the lunar eclipse data taken at BBSO on November 29, 1993, as discussed in the previous section. The lunar phase function for the bright side, $f_b(\theta)$, is used in the formula to account for the geometrical dependence of the reflectivity of the moon, while $f_a(\theta_0)$ accounts for the fact that the earthshine is not exactly retroflected from the moon ($\theta_0 \lesssim 1°$). In our analysis, θ_0 is taken as the angle between the observer's position and the mean of the sub-solar point (position on the earth's surface of the solar zenith) and the sub-lunar point (position on the earth's surface of the moon's zenith) with the apex of the angle being defined with respect to the fiducial patch under consideration, see Figure 1. We assume that the moonshine and earthshine have the same lunar phase function for each fiducial patch. Thus, we take $f_a(\theta_0)$ from the appropriate moonshine phase function. The earthshine is slightly bluer than the moonshine because of Rayleigh scattering by the earth's atmosphere. This small effect is subsumed in the lunar geometrical albedos.

From Equation (28), one may surmise that the observational errors arising from measuring A^* from two opposing fiducial patches come from the errors in the readout intensity from the moonshine and earthshine fiducial patches, the error in the transmission of the BS filter (about 0.8%), and the error in the determination of lunar phase function. The ratio $\frac{p_b}{p_a}$ can be regarded as the relative normalization of the phase functions of the opposing fiducial patches. The standard deviation of the lunar phase function can be determined down to 0.5% from a co-variance calculation with a comparable uncertainty for the ratio $\frac{p_b}{p_a}$. The standard deviation of the Beer's law fitting of the moonshine for each night is taken as the error of the moonshine intensity. This gives a value of 1.1%. For the case of the earthshine, the scattering of the data is due to both the noise and the real physical changes in the terrestrial albedo. The average standard deviation from Beer's law fitting of the earthshine intensities is 1.9%. Conservatively speaking, if half the amount of such scattering comes from the real physical change on average, the error in nightly earthshine intensity measurement is about 1.0%. Adding up all the errors and assuming they are independent, we get a nightly measurement error of nearly 2%. If one regards the measurements from different pairs as being independent, the 2% is reduced to about 1%.

The precise determination of the effective albedo for one night cannot yield a bond albedo; rather, one needs to integrate the effective albedo for many nights (over as wide a range of lunar phase angles as possible). If we combine nights to obtain, say, a seasonal average, then the total error will be smaller, but no smaller than that associated with the mean values of the various lunar phase functions and their relative normalizations. We regard the determination of the ratio $\frac{p_b}{p_a}$ as being the most likely source of systematic errors. Measurements of the opposition effect in future eclipses will allow us to determine if there are systematic errors, and correct the albedos in retrospect.

To determine the Bond albedo, A, from our earthshine observations we need to integrate $A^*(\theta)$ over all phases of the moon. Combining Equations (6), (7) and (9), we find

$$A = \frac{2}{3}\int_{-\pi}^{\pi} d\theta A^*(\theta) f_L(\theta)\sin\theta. \qquad (29)$$

There are two basic problems using this approach to determine the Bond albedo. The first, and more significant problem, is that we cannot measure the earthshine for all phases of the moon. This becomes a problem primarily for lunar phases near the new moon, where the earth is most nearly Lambertian. The second basic problem in using the earthshine to determine the albedo arises because the orbit of the moon traces out an ellipse in the full three dimension space surrounding the earth, so we cannot measure the earthshine in all directions. Therefore, we are insensitive to any azimuthal anisotropy in the earthshine. In the following paper of this series, we will demonstrate that the anisotropy is not significant, and one can account for it. We do this by taking advantage of full spatial coverage provided by the simulations. For the first problem, we will show that we can obtain a quite reliable Bond albedo from the earthshine data. These are among the subjects of Paper II of this series.

Appendix A: Earthshine Instrumentation and Data Acquisition

Earthshine observations are currently being carried out at BBSO. The earthshine telescope is aligned with, and mounted atop the 65 cm solar telescope. Figure 13 shows a schematic of the earthshine telescope.

.1.1. Hardware

The basic optical components of the earthshine telescope consist of an f/15 telescope primary, which is a 15 cm diameter air-spaced doublet. The telescope tube is attached and aligned with the 65 cm solar telescope, which enables us to use the large telescope's drive software, permitting tracking following the moon's variable rate. The tracking rate is updated, via software, every thirty minutes to match the changing lunar motion in the east-west direction. Minor north-south corrections are done with the telescope control paddle as needed during the course of the night's observations. The 65 cm telescope is regularly re-balanced for equipment changes so that tracking stability is not a problem even with long exposures. At the end of the tube is a stray light field stop. The incoming moonlight passes the

field stop, and then enters a light-tight optical assembly box that holds the filters and camera optics.

In the box, just behind the tube field stop and just before prime focus, is the earthshine neutral density filter switcher. Two filters are placed in the switcher. The first neutral density filter is a Schott NG3 2mm (the laboratory measured transmission of the filter, used for the first two years of observations, is 0.0115, as a whole, from 4000-7000 Å) for the bright side (BS) measurements. The BS or moonshine filter covers the entire field of view and is in place to prevent camera saturation and to provide a reasonably long exposure time (several 100 ms) compared to the smallest exposure time for the camera (10 ms). Thus, to determine the absolute value of the earth's reflectance, one needs to know precisely the transmission of this filter (§4.3). The second filter is a Schott NG10 2mm (transmission is about 2×10^{-5} over 4000-6000Å, although its precise value is irrelevant for our observations), which is essentially a blocking filter to cut off the bright side of the moon to permit the dark side or earthshine (ES) observations. The blocking filter covers the bright side of the moon to permit long, dark side exposures (~60-150 s) to get optimal signal to noise for the ES images. The blocking filter is carefully placed within the filter holder, by hand, at the beginning of each observing session. Its location, designed to cover the terminator, depends on the phase and libration of the moon.

The prime focus is after the filter holder, and it is closely followed by a flat field lens. Next in the optical train are two near IR filters, which stop any light beyond 7000 Å from reaching the camera. An iris behind the near IR filters acts as a further stray light stop. Behind the iris is a camera lens that focuses the lunar image on the CCD. Between this lens and the camera is a space for a second filter wheel (not shown), which can be used for narrow band measurements. All elements are rail mounted for linear adjustments, and lens elements are in moveable $y - z$ mountings for fine adjustments. All fine-tuning was done in the Fall of 1998, and nothing has been changed on the system since the start of data acquisition in December 1998. The system was "frozen" to limit possible errors in calibrating the lunar phase function. Flat field images help to point out the location of occasional dust particles that get into the optics. Compressed air removes most particles, and when necessary, elements are removed for cleaning, and then are carefully replaced to preserve optical alignment.

The CCD camera used in our current earthshine observations is an Apogee 7. The camera is a 512 X 512 16-bit scientific system with a SITe back-illuminated, thinned silicon chip. This chip, which is one of SITe's highest grade, is designed for higher quantum efficiency than unthinned front illuminated chips – this advantage is most apparent toward the blue. One drawback of the higher efficiency SITe chip is its sensitivity to "after-images" caused by exposure to UV. Testing the earthshine system to limit this effect resulted in the following observing procedures: 1) The UV from the BS images is reduced by the BS (NG3) filter. 2) The worst after-images show up in the ES images on the unfiltered half of the image – which are of long exposure. It was found that a series of subsequent, short BS images, the UV residual image was removed before the next long earthshine exposure. 3) Careful examination of dark current and flat field images taken during the course of observations is done to confirm this, night by night.

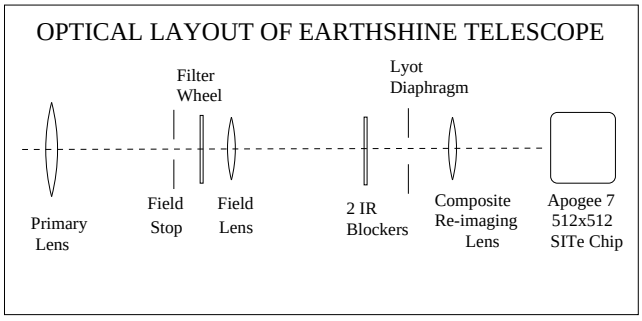

Figure 13. The optical set-up of the earthshine telescope.

Initial testing demonstrated a linear response over the camera's entire 16-bit range. To check for change in the camera's response with time, a calibrated radiometer was purchased to check the camera's response during each new moon. Dome flats are taken in varying illumination to get pixel count versus intensity. The radiometer is an IL 1700, a NIST traceable Silicon photodiode radiometer. Once a year, the radiometer will be returned to International Light for re-calibration.

.1.2. Observations

After initial tests, our current round of earthshine observations began in November 1998. A typical raw image is shown in Figure 2. The five pairs of fiducial patches used in the data reduction (see section 3) are also indicated. The camera's graphic user interface, in C code, was supplied by the manufacturer, and it was modified to efficiently handle the routine earthshine observations. The nightly observations follow a simple set of procedures, which are mostly automated. During the course of observations BS, ES, dark current, and flat field images are taken regularly.

The first 8 months of observations covered lunar phases between 0° and ±140°, which is about 21 days a month. The initial observation over this wide range of phases was necessary to determine the lunar phase function and prove its repeatability. During the first 8 months, for the phases near the full moon (-40° through 0° to +40°), ES images were not taken because both fiducial patches were in, or so near to sunlight that ES measurements were unreliable (see cartoons in Figure 1). On these nights only BS, dark current, and flat fields, were taken to determine the scattering of light from the fiducial patches as a function of the phase of the moon. The lunar phase function was determined by July 1999, so that the BS only nights were dropped – except for observations of the full moon. Full moon observations are still taken to determine the role of the opposition effect (Flatté et al. 1991) in the lunar phase function (phases -15° to +15°). Current earthshine observations cover about 14 days per month, and cover lunar phases between ±40° to ±150° centered on the first and last quarters of the moon when we have optimal conditions for measuring the earthshine – close to full-earth with a few hours of observations being possible. Data rates vary depending on phase. An average night will give about 1 image per minute. This means that the number of raw images saved for data reduction, varies between 100 to 600 per night.

Appendix B: Measuring the Transmission of the Bright Side Filter

A precise determination of the earth's reflectance from observing the moon depends on an accurate measurement of

the ratio of the true earthshine intensity to the true moonshine intensity. This determination is complicated by the fact that the moonshine is so bright that when we measure it, we must use a filter (see Figure 2) that reduces the intensity of the moonshine by about 99%. The reduction enables us to have a reasonably long exposure time (of order a few 100 ms) compared to the shortest possible exposure time of the camera (10 ms). When we observe the earthshine, the moonshine or BS filter is removed and the much stronger, blocking filter is inserted to block the moonshine to prevent camera blooming during the much longer exposures. Thus, to know the true ratio of the earthshine to moonshine intensity, we must also precisely determine the transmission of the moonshine filter at the point through which the moonlight passes (point-to-point variations could well be significant). This fact became abundantly clear after October 13, 2000 when the original filter was destroyed, and was replaced by one that was comparable in the lab specifications for the transmission over the whole filter. Initially, we assumed that the transmission of the new filter was the same as the old one. However, we found that the observed moonshine intensity noticeably increased, indicating that the new filter has a significantly larger transmission than the old filter.

In the observations, the moonshine filter, MS, is placed at a fixed position in the focal plane covering the entire lunar image, so that the light always passes through the same point on the filter. This is important because there is some point-to-point variation in the transmission of the filter. In our effort to precisely determine the transmissions of the old and new BS filters at the focal point of the lunar image, we first employed identical approaches for both of the filters. To measure the transmission of the old filter, we re-analyzed thirty nights of moonshine and earthshine data that we had in-hand for nights near the new moon - where the earthshine signal is most intense. To illustrate the reanalysis procedure, one can look at Figure 14 for guidance. For that night, with the old filter, we measured the total earthshine intensity in five parallel strips, somewhat wider than the fiducial patches and running from the earthshine fiducial points toward the moonshine crescent. In that figure, the five strips are shown together as a striped, bright, four-cornered patch. Each strip in the bright patch runs from the edge of the moon and is 5° wide in latitude and 30° long in longitude. That way, each strip would have a statistically significant number of counts in the earthshine region, even for the relatively short exposure times of a few hundred milliseconds, used on that, and other nights, for each data point with the BS filter in place (but without the much stronger blocking filter in place). The lunar phase in Figure 14 is +134°. Large magnitude phase angles are chosen so that the earthshine is the brightest, while the stray light the smallest. The determination of the transmission of the old BS filter is shown for that typical night in Figure 15. The dark side of the moonshine and the earthshine intensities are each extrapolated to zero airmass, and corrected for the small effect of stray light, (as described in §4.1), and their ratio yields a transmission of 0.0114±0.005 for that night. The error weighted mean transmission for all thirty nights is 0.01127±0.00011 for the old filter. Implicit in this approach to determining the broadband transmission of the filter is the assumption that the spectrum of the earthshine and moonshine are roughly the same; this assumption works here because the transmission curve of the filter is flat over visible wavelengths. Most of the noise in the result arises from the short exposure time for the MS filter covered observations. The 0.01127±0.00011 is within the factory quoted errors of the 0.0115 value given by Schott.

For the new filter, we have re-analyzed twelve nights of data in the same way and find a transmission of 0.01338±0.00017 for the focal point, whereas the factory-reported average across the filter is 0.0114. The latter transmission is nearly identical to that of the old filter, but quite far from 0.01338±0.00017. The larger transmission at the focal point accounts for the apparent rise in moonshine intensity after October 13, 2000. We will continue collecting more data on the transmission using future data. However, we have a more powerful and more precise cross-check in hand – using lunar phase function data on the crescent and moonshine, which we know to 0.5%.

Analyzing all of our good nights of moonshine observations, with the new and old new filter, at all phases, we have constructed for each a lunar phase function – the change in brightness with lunar phase for the moonshine and crescent intensities. From all these nights, we have selected the nights during the period for which the old filter was used, and then we calculated a second-degree polynomial fit to the lunar phase data. The data for these nights have been reduced using a transmission value of 0.01127. After that, we analyze the phase function for the nights taken with the new filter and calculate the standard deviation of the values to the lunar phase function fit to the old data, but leave the new filter transmission as a variable.

Our procedures consist of multiplying the intensities of the new phase function data by a factor between 0.9 to 1.4 in steps of 0.0001, and for each case calculating the standard deviation to the old data fit. The agreement of the

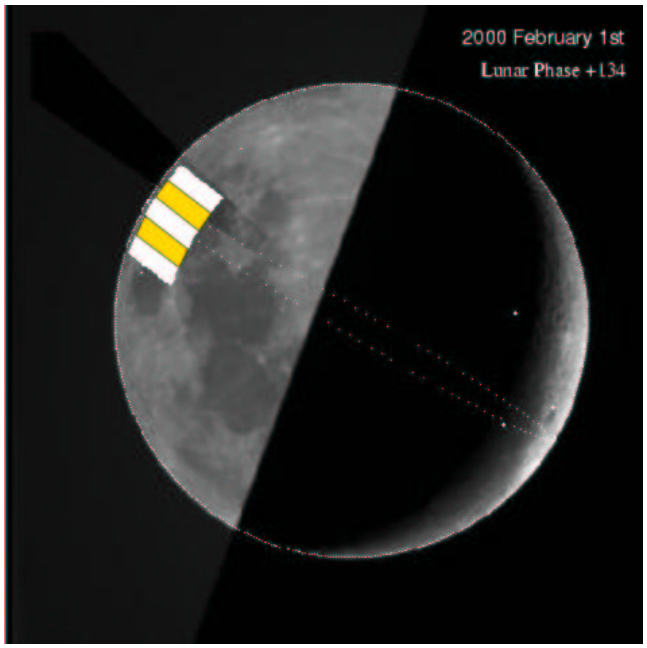

Figure 14. This image of the earthshine on the night of February 1, 2000 shown is one with the blocking filter, which enables long exposures of the earthshine. The bright, rectangular patch indicates the area of five strips used to compare the earthshine intensity with and without the moonshine filter (BS filter), so as to determine the transmission of the BS filter. The lunar phase was +134° that night, and so the earthshine signal is relatively strong. The crescent is not visible through the strong blocking filter in the original image, but has been restored here for reference.

new data with the fit to the old data will be optimal when the standard deviation is minimized.

We find the best agreement between the two lunar phase functions when the transmission of the new filter is 0.0132 (0.01319 for the moonshine and 0.01322 for the crescent). This is excellent agreement with the transmission determined from the first method. Thus, we have precisely determined the transmission of the new filter to the same precision as the old filter, so that we use 0.0132±0.0001 as its transmission after including errors in the phase function. As we gather more data on the new filter, we can determine its transmission to the same precision to which we know the lunar phase function, and then the error on the transmission can be reduced to about ±0.00005. Following that, we can use this information to reduce the quoted precision of the old filter to that for the lunar phase function determined for the old filter.

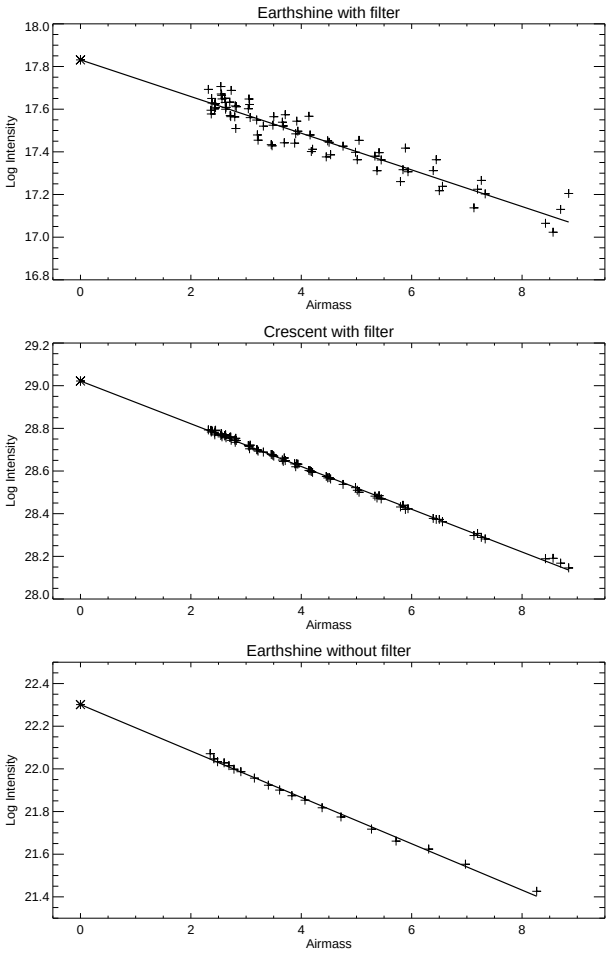

Figure 15. The upper panel shows the observed, BS filter-blocked earthshine intensity as a function of airmass on February 1, 2000. The "+" signs in that panel represent the intensity of one of the stripes. The linear fit to the data has been extrapolated to zero airmass with that result being indicated by the asterisk, which is the left-most mark on the fit. The lower panel shows the same type of data, but without the BS filter. The ratio of the two intensities, for that night, extrapolated to zero airmass, and corrected for the small effect of stray light, implies a MS filter transmission of 0.0114±0.0005. The lunar phase that night was +134°.

Acknowledgments. This research was supported in part by a grant from NASA (NAG5-11007).

References

Allen, C. W., *Astrophysical Quantities*, A.N. Cox (ed), AIP Press (Springer-Verlag), New York, ISBN 0-387-98746-0, p.125, 1973.

Arnold, L., s. Gillet, O. Lardiére, P. Riaud, J. Schneider, A test for the search for life on extrasolar planets, *Astronomy & Astrophysics*, 392, 231-237, 2002.

Betts, R.A., Offset of the potential carbon sink from boreal forestation by decreases in surface albedo, *Nature*, 408, 187-190, 2000.

Buratti, B.J., J.K. Hillier, and M. Wang, Icarus, 124, 490-499, 1996.

Cess, R.D., and 33 co-authors, Cloud feedback in atmospheric general circulation models: an update, *Journal of Geophysical Research*, 101(D8), 12791-12794, 1996.

Charlson, R.J., S.E. Schwartz, J.M. Hales, R.D. Cess, J.A. Coakley Jr, J.E. Hansen, D.J. Hofmann, Climate forcing by antropogenic aerosols, *Science*, 255, 423-430, 1992.

Danjon, A., Recherches sur la photométrie de la lumière cendrée et l'albedo de la terre, *Ann. Obs. Strasbourg*, 2, 165-180, 1928.

Danjon, A., Albedo, color, and polarization of the earth, *The Earth as a Planet*, ed. Kuiper, Chicago, 726-738, 1954.

Dubois, J., Sur l'albedo de la terre, *Bull. Astron.*, 13, 193-196, 1947.

Eddy, J., The Maunder Minimum, *Science*, 192, 1189-1202, 1976.

ERBE Data Management Team, ERBE Data Management System, Earth Radiant Flux and Albedo, Scanner S-9, Nonscanner S-10 User's Guides. NASA/Langley, Hampton, Virginia, 1985.

Flatte, S., S.E. Koonin., and G. MacDonald, *Global Change and the Dark of the Moon*, JSR-91-315 (McLean, VA: The MITRE Corporation), 1991.

Franklin, F.A., Two-Color Photometry of the Earthshine, *J.Geophys.Res.*, 72, 2963-2967, 1967.

Fritz, S., The albedo of the planet earth and of clouds, *J. Meteor.*, 6, 277-282, 1949.

Fröhlich, C., Observations of irradiance variations, *Space Science Reviews*, v. 94, 15, 2000.

Goode, P.R., J. Qiu, V. Yurchyshyn, J. Hickey, M.C. Chu, E. Kolbe, C.T. Brown, and S.E. Koonin, Earthshine observations of the earth's reflectance, *Geophys. Res. Lett.*, 28 (9), 1671-1674, 2001.

Goode, P.R., E. Pallé, V. Yurchyshyn, J. Qiu, J. Hickey, P. Montañés Rodriguez, M.C. Chu, E. Kolbe, C.T. Brown, and S.E. Koonin, Earthshine and the earth's albedo II: Observations and simulations over three years, *submitted*, 2003.

Hapke, B., Physics and Astronomy of the Moon, 2nd edition, ed. Z. Kopal, Academic Press, New York, 155, 1971.

Hapke, B.W., Nelson, R.M., and Smythe, W.D., The opposition effect of the moon - the contribution of coherent backscatter, *Science*, 260, 509-511, 1993.

Hapke, B., Nelson, R., and Smythe, W., The opposition effect of the moon: coherent backscatter and shadow hiding, *Icarus*, 133, 89-97, 1998.

Helfenstein, P., Veverka, J., and Hillier, J., The lunar opposition effect: A test of alternative models, *Icarus*, 128, 2-14, 1997.

Houghton, J., The physics of atmospheres, 3rd edition, Cambridge University Press, CAmbridge, pp 320, 2002.

Huffman, D., C. Weidman, and S. Twomey, *Colloq Andre Danjon*, Jounees 1990, Capitaine and Detarbat, eds. (Paris: Paris Observatory), p. 111, 1990.

Intergovermental Panel on Climate Change (IPCC), 1995, Climate Change 1994, *Radiative Forcing of Climate Change and an Evaluation of the IPCC 1992 Emission Scenarios*, ed. J.T. Houghton, L.G. Meira Filho, J. Bruce, H. Lee, B.A. Callender, E. Haites, N. Harris, K. Maskell, Cambridge, MA: Cambridge University Press, 1994.

Jayne, S.R., and J. Marotzke, The Dynamics of Ocean Heat Transport Variability, *Reviews of Geophysics*, 39, 385-411, 2001.

Kennedy, J.R., M.S. Thesis, Fresno State College, unpublished, 1969.

Lean, J., The sun's variable radiation and its relevance for earth, *Ann. Rev. Astron.*, 35, 33, 1997.

Liou, K.N., An introduction to atmospheric radiation, second edition, *International Geophysics series*, 80, R. Dmowsca, J.R. Holton and H.T. Rossby (eds), Acdemic Press, Elsevier Science, 2002.

Pallé, E., P.R. Goode, J. Qiu, V. Yurchyshyn, J. Hickey, P. Montañés Rodriguez, M.C. Chu, E. Kolbe, C.T. Brown, and S.E. Koonin, Earthshine and the earth's albedo III: Long-term variations in reflectance, *submitted*, 2003.

Randall, D.A., and 26 more authors, Analysis of snow feedbacks in 14 general circulation models, *Journal of Geophysical Research*, 99(D10), 20757-20771, 1994.

Ram, M., and M.R. Stoltz, Possible solar influences on the dust profile of the GISP2 ice core from Central Greenland, *Geophys. Res. Lett.*, 26, No. 12, 1763, 1999.

Ramanathan, V., R. D. Cess, E. F. Harrison, P. Minnis, B. R. Barkstrom, E. Ahmad, and D. Hartmann, Cloud-Radiative Forcing and Climate: Results from the Earth Radiation Budget Experiment, *Science*, 243, 57-63, 1989.

Ridley J., Variations in planetary albedos', *4th annual ROE Workshop*, Royal Observatory Eddimburgh, ed W.R.F. Kent, 2001.

Seiji, K., N.G. Loeb, and C.K. Rutledge, Estimate of top-of-atmosphere albedo for a molecular atmosphere over ocean using Clouds and the Earth's Radiant Energy System measurements, *Journal of Geophysical Research*, 107 (D19), 4396, doi:10.1029/2001JD001309, 2002.

Tikhoff, G.A., *Mitteilungen der Nikolai-Hauptsternwarte zu Pulkovo*, No. 62, Band VI_2, 15, 1914.

Ueno, S., In *Processes in marine remote sensing*, University of South Carolina Press, P.J Vernberg and F.B. Diemer (eds), 12, 459-509, 1981.

Willson, R.C. and H.S. Hudson, Solar luminosity variations in solar cycle-21, *Nature*, 332, 810, 1988.

Willson, R.C. and H.S. Hudson, The suns luminosity over a complete solar-cycle 1991, *Nature*, 351, 42, 1991.

Woolf, N.J., P.S. Smith, W.A. Traub, and K.W. Jucks, The Spectrum of Earthshine: A Pale Blue Dot Observed from the Ground, *Astrophysical Journal*, 574, 430-433, 2002.

Big Bear Solar Observatory, New Jersey Institute of Technology, Newark, NJ 07102, USA

(Received _____.)

Figure 1:A not-to-scale cartoon of the sun-earth-moon system viewed from the pole of earth's orbit. In the top panel, the earth's topocentric phase angle, α, with respect to BBSO is defined. The plot also shows the moon's selenographic phase angle, θ, with respect to one of the fiducial points (Grimaldi) used in the observations made from BBSO (also indicated). β is the angle between the sunlight that is incident somewhere on the earth and reflected, as earthshine, to Grimaldi. $\theta_0(=\beta-\alpha)$ is the angle between the earthshine that is incident, and reflected from the moon. The path of the earthshine is indicated by the arrows. θ_0 is of order 1°, or less. In the lower panel the same diagram is drawn for a negative lunar phase angle, and extra features like the moon's orbit around the earth are indicated. On both panels the aspect of the moon as would be seen from BBSO is also indicated in a box. The light-shaded areas of the earth indicate the aproximate latitude range that contributes to the earthshine. Note how for positive lunar phases (top panel) the earthshine contribution comes from latitudes west of BBSO while for negative phase (lower panel) angles it comes from latitudes east of BBSO.

Figure 2: The moon showing the bright side and the earthshine. The Grimaldi side is in the moonshine and the Crisium side is in the earthshine. Our ten fiducial patches used in the observations made from BBSO are indicated. The crosses give the approximate positions of Danjon's fiducial patches. Goode et al. (2001) used one fiducial patch on each side, and on the Crisium side it is the one closest to the white cross, while on the Grimaldi side, it is the one immediately above the black cross. In the image, the lunar phase is 115°.9, near a declining quarter moon. Unlike the moonshine, the earthshine is flat across the disk. The flatness is due to the uniform, incoherent back-scattering (non-Lambertian) in contrast to the forward scattering of sunlight occuring in the sunlit lunar crescent surface.

Figure 3: Illustration of the background subtraction for earthshine images. The image on the left shows a background cone around a fiducial patch, within which the intensity of the background points are read out to make a fit as a linear function of the distance from the lunar center. For the image shown, the intensity inside the cone has the background subtracted already. The plot on the right shows the decline of the off-limb intensity as the background point gets further from the lunar center, and the overplotted thick grey line indicates the least-square linear fit.

Figure 4: In each of the four tryptics of the figure the intensity per unit (lunar) area of the moonshine (top panel), the crescent (middle panel), or the earthshine (bottom panel), is plotted against time (on the left) and airmass (on the right). These intensities are data count values read from the CCD, corrected for all the steps indicated in section 3.1, and divided by the lunar phase function. In the case of moonshine and crescent intensities, the value has been also divided by the transmission of the bright side filter. The "+"'s indicate observed data points, and the solid lines are the fits to Beer's law. *Upper six panels:* data from the night of September 5, 1999, demonstrating a typical good night, and the standard deviation of the fitting is 0.007, 0.005, 0.007 (from top to bottom). *Lower six panels:* data from the night of September 17, 1999, demonstrating a typical, partly cloudy night, and the standard deviation of the fitting is 0.219, 0.183, 0.077 (from top to bottom).

Figure 5: The moonshine, crescent and earthshine intensities and their Beer's law fit for the night of 2000 January 28, showing that while the moonshine and crescent intensities follow Beer's law very well, the earthshine intensity evolution deviates from Beer's law. The standard deviations of the fits are 0.004, 0.005, 0.014, respectively. The fact that the fit is poor only for the earthshine implies sizeable short-term variations in the earth's effective albedo as seen from BBSO due to a combination of factors including, among others, the earth's rotation, anisotropic reflectance and weather changes.

Figure 6: The variation of the atmospheric extinction coefficients for the crescent, (α_c), moonshine (α_m) and earthshine (α_e). Panel (a) illustrates α_m (for five fiducial patches as indicated by different symbols) against α_c from which it is clear that the crescent and moonshine patches are very much alike; (b) shows α_m of four out of five fiducial patches (as indicated by different symbols) vs. the fifth fiducial patch, illustrating that α_m is virtually the same for different patches (note the equivalence of each linear, least squares fits to the data for each patch); (c) shows α_e for four out of five fiducial patches (as indicated by different symbols) vs. the other fiducial patch, showing that α_e is also the same for different fiducial patches in the earthshine; and (d) shows α_e (of all fiducial patches in earthshine) against α_c, which is consistent with the earthshine being bluer than the moonshine. The various straight lines in each panel indicate a least squares fit to the appropriate data.

Figure 7: The intensity of the *moonshine* for the Crisium side and Grimaldi side fiducial patches of Goode et al. (2001) with a third order polynomial (including higher order terms has no noticeable effect) fit for each. Clearly, there is a roughly linear decrease in the intensity of the reflected light going from full moon to new moon.

Figure 8: The deviation of the moonshine fiducial patch intensity from average against the deviation of the overall intensity of the crescent. Left: data points from morning observations of Grimaldi; right: data points from evening observations of Crisium. The solid lines in each panel show the linear fit to each cluster of points.

Figure 9: The deviation of the moonshine fiducial patch intensity (after the first and second step corrections) from average against the deviation as a fitting result from Equation (25). Left: data points from morning observations; right: data points from evening observations.

Figure 10: Fit of lunar eclipse data obtained on November 29, 1993. (a) Beer's law fit of the Crisium side (Equation 19); (b) Composite Beer's law plus opposition effect fit on the Crisium side (Equation 27); (c) same as (a) on the Grimaldi side; (d) same as (b) on the Grimaldi side.

Figure 11: The top panel shows the apparent, relative lunar phase function from the raw data, for which there are points down to 2°. The function is made relative by normalizing it to unity at phase angle 0°, which means that the ratio of the true right and left branch intensities yields the ratio of the geometrical albedos between Crisium and Grimaldi. The peak near small phase angles represents the opposition effect. Data from a total eclipse are used to connect the positive and negative phase branches of the lunar phase function. No eclipse data are shown in this figure, but the result of the eclipse data is the opposition peak. The second panel from the top shows the result after including correction for the local atmospheric effects using the lunar crescent as a guide star. The third panel also includes the correction for lunar declination. The fourth panel includes the correction for lunar libration. The fit shown in each

panel is the final one resulting from all of the corrections described in section 5.

Figure 12: Danjon's phase function (solid line) is plotted against lunar phase. Using Figure 11d, the dashed line is our phase function for evening observations and the dotted line for morning for the fiducial patch of Figure 11.

Figure 13: The optical set-up of the earthshine telescope.

Figure 14: This image of the earthshine on the night of February 1, 2000 shown is one with the blocking filter, which enables long exposures of the earthshine. The bright, rectangular patch indicates the area of five strips used to compare the earthshine intensity with and without the moonshine filter (BS filter), so as to determine the transmission of the BS filter. The lunar phase was $+134^\circ$ that night, and so the earthshine signal is relatively strong. The crescent is not visible through the strong blocking filter in the original image, but has been restored here for reference.

Figure 15: The upper panel shows the observed, BS filter-blocked earthshine intensity as a function of airmass on February 1, 2000. The "+" signs in that panel represent the intensity of one of the stripes. The linear fit to the data has been extrapolated to zero airmass with that result being indicated by the asterisk, which is the left-most mark on the fit. The lower panel shows the same type of data, but without the BS filter. The ratio of the two intensities, for that night, extrapolated to zero airmass, and corrected for the small effect of stray light, implies a MS filter transmission of 0.0114 ± 0.0005. The lunar phase that night was $+134^\circ$.